Maya G Kopylova*, Yvette Beausoleil, Alexey Goncharov[1], Jennifer Burgess[2**], Pamela Strand[2 ***]

Spatial distribution of eclogite in the Slave cratonic mantle: The role of subduction

University of British Columbia, 2207 Main Mall, Vancouver, Canada V6T1Z4

[1] – Institute of Earth Sciences, St-Petersburg State University & IPGG RAS, 2 Makarova, 199034, Saint-Petersburg, Russia

[2] – Shear Minerals Ltd., 220 - 17010 – 103rd Ave, Edmonton, AB Canada, T5S 1K7

Revised for Tectonophysics

November 2015

corresponding author, mkopylov@eos.ubc.ca

** - present address: Burgess Diamonds, 5674 Annex Road, Sechelt, BC, Canada, V0N 3A8

*** - present address: NWT Mines and Minerals, Box 1320, 4601B 52nd Ave, Yellowknife, NT, Canada, X1A2L9

Abstract

We reconstructed the spatial distribution of eclogites in the cratonic mantle based on thermobarometry for ~240 xenoliths in 4 kimberlite pipes from different parts of the Slave craton (Canada). The accuracy of depth estimates is ensured by the use of a recently calibrated thermometer, projection of temperatures onto well-constrained local peridotitic geotherms, petrological screening for unrealistic temperature estimates, and internal consistency of all data. The depth estimates are based on new data on mineral chemistry and petrography of 148 eclogite xenoliths from the Jericho and Muskox kimberlites of the northern Slave craton and previously reported analyses of 95 eclogites from Diavik and Ekati kimberlites (Central Slave). The Northern Slave eclogites of the crustal, subduction origin occur at 110-170 km, shallower than in the Central Slave (120-210 km). The identical geochronological history of crustal Slave eclogites and the absence of steep suture boundaries between the central and northern Slave craton suggest the lateral continuity of the mantle layer relatively rich in eclogites. We explain the distribution of eclogites by partial preservation of an imbricated and plastically dispersed slab formed by easterly dipping Proterozoic subduction. The depths of eclogite localization do not correlate with geophysically mapped discontinuities. The base of the depleted lithosphere of the Slave craton constrained by thermobarometry of peridotite xenoliths coincides with the base of the thickened lithospheric slab, which supports contribution of the recycled oceanic lithosphere to formation of the cratonic root. Its architecture may have been protected by circum-cratonic subduction and shielding of the shallow Archean lithosphere from the destructive asthenospheric upwelling.

Key words: Slave craton, eclogite, subducted slab, thermobarometry, anisotropy, seismic discontinuity

Highlights

- Depth distribution of eclogites below the Slave craton is reconstructed from kimberlite-borne xenoliths
- The Northern Slave eclogites of the crustal, subduction origin occur at 110-170 km, shallower than in the Central Slave (120-210 km).
- Preservation of a laterally continuous thickened slab formed by easterly-dipping Proterozoic subduction

- The deep limit of the eclogite distribution coincides with the base of the Slave depleted lithosphere
- Circum-cratonic subduction may control localization of eclogites and the geometry of the lithospheric root

1. Introduction

Eclogites are an important part of the cratonic mantle. They are interspersed with the predominant mantle peridotites during cratonic root formation by subduction-related melting processes and tectonic imbrication of the oceanic slab (Pearson and Wittig, 2008). Eclogites may be added by subduction to the periphery of the already stabilized cratonic mantle (Shirey et al., 2003; Helmsteadt, 2009; Aulbach, 2012). Moreover, mantle melting may also result in eclogite formation *in situ* (e.g. Barth et al., 2002). All these processes should lead to distinct spatial distribution of eclogites in the cratonic root. The distribution, therefore, can be used to infer processes of the cratonic growth.

The goal of our study is to reconstruct the spatial localization of eclogites in the Slave cratonic mantle. This craton in the western Canadian Shield (Fig. 1) has a well constrained geological history (Snyder, 2008; Helmsteadt, 2009) and a thoroughly studied mantle, mapped geophysically (e. g. Snyder et al., 2004; 2014) and petrologically (e. g. Kopylova and Caro, 2004; Heaman and Pearson, 2010). The long sequence of tectonomagmatic events pre- and post-dating craton stabilization is mirrored in the complex architecture of the Slave mantle, which is compositionally stratified, separated in multiple domains and hosts zones distinct in geophysical and geochemical properties.

We characterized depth distribution of eclogites with known origins from various parts of the Slave craton using a consistent thermobarometric approach. Our work, which ties all eclogites of one craton into a single 3D network, is complementary to petrological studies of eclogites that focus usually on mineralogy, trace element chemistry and geochronology of selected few samples (Heaman et al., 2006; Schmidberger et al., 2007; Aulbach et al., 2007; 2011; De Stefano et al., 2009; Smart et al., 2014). The majority of the new data is collected for 150 eclogite xenoliths from the Northern Slave pipes Jericho (Kopylova and Hayman, 2008) and Muskox

(Hayman et al., 2008; Newton et al. 2015). These Jurassic (172.1 ± 2.4 Ma; Heaman et al., 2006) pipes belong to the same cluster and situated only 15 km apart. The mineral compositions and thermobarometric estimates for the Northern Slave eclogites are compared to the respective datasets for Central Slave eclogites from Diavik and Ekati kimberlites,150 km southeast of the Jericho-Muskox kimberlite cluster, in the center of the craton (Fig. 1). Our analysis led to conclusions on the role of subduction in the build-up of deep cratonic roots, the localization of eclogites in the mantle and the geometry of the cratonic lithosphere.

2. Origin of cratonic eclogites

Eclogite is a common lithology among kimberlite-derived mantle xenoliths. The eclogites from the cratonic mantle are generally assigned “crustal” or “mantle” origin. The most common crustal origin involves two stages of rock formation, 1) generation of basalts and gabbros by shallow mantle melting in mid-ocean ridges, and 2) subduction and metamorphism of the crustal mafic rocks at mantle depths (Jacob, 2004). The alternative is the *in situ* mantle origin, whereby mantle mafic melts cannot escape to the crust and thus crystallize at depth into the clinopyroxene-garnet assemblage (e.g. Barth et al., 2002).

The crustal or mantle origin of eclogite is inferred based on bulk and mineral compositions, which ideally should be combined with trace element and O isotope data. The latter geochemical characteristics, however, rarely are available for many samples, hampering unequivocal conclusions on the eclogite origin. To address this problem, several approaches have been used. Based on the correlation between the geology of the eclogite-bearing terrane and the mineral chemistry of the eclogites, they were classified into Groups A, B, and C, with the mantle Group A eclogites, and the crustal origin of the Group B/C eclogites (Coleman, 1965; Taylor and Neal, 1989). This simple principle has been further justified by comparison of whole-rock compositions with assumed protoliths, reconstructed whole rock REE patterns, Sr-Nd systematics and $\delta^{18}O$ signatures (Neal et al., 1990; Snyder et al., 1997). For example, 14 diamondiferous eclogites from Udachnaya (Siberian craton) that belong to Group B/C were inferred to be former ocean floor basalts based on reconstructed REE and bulk compositions of the protoliths (Jerde et al., 1993b). Koidu eclogites (Man Craton, West Africa) show a contrast between high-Mg eclogites with Group A garnets and low-Mg eclogites classified as Group B/C

(Barth et al., 2001, 2002). Only Group B/C eclogites demonstrate stable oxygen isotopes outside of the mantle values and therefore was interpreted as ancient altered oceanic crust that underwent partial melting during subduction. All Group C eclogites and a part of Group B eclogites have low-Mg whole rock composition (6-13 wt% MgO) and typically contain accessory kyanite and quartz, the hallmarks of crustal origin (Barth et al., 2001, 2002).

In some other suites of kimberlite-derived eclogites, correlations between stable oxygen isotopes and the sample mineralogy, and between the major and trace element chemistry is absent (Snyder et al., 1997; Riches et al., 2010). For these suites, samples of the crustal or mantle origin randomly fall into Groups A, B, C and parameters other than the mineral chemistry should be used as a predictor for the protolith. Commonly, these are Eu and Sr anomalies, HREE contents and the oxygen stable isotopes (Jacob, 2004).

3. Eclogite xenoliths in kimberlites of the Slave craton

Eclogite xenoliths occur in many kimberlites of the Slave craton, but only in the Jericho, Diavik and Ekati pipes the eclogites are extensively studied.

In Jericho, where the total population of mantle xenoliths has been assessed, eclogites comprise 25.4% (based on 3216 xenoliths), being the second most abundant rock type after peridotite (Kopylova et al., 1999a). Jericho eclogites have been classified using several different criteria into 1) Groups A, B, C (Kopylova et al., 1999a, Heaman et al., 2006; Smart et al., 2014), 2) foliated and massive types (Kopylova et al., 1999a; De Stefano et al., 2009); 3) diamond-bearing and zircon-bearing (Heaman et al., 2006); and 4) high-Mg, peaked, depleted, and sloped (Smart et al., 2014). The general consensus is that the majority of Jericho eclogites are crustal in origin (Heaman et al., 2006; De Stefano et al., 2009; Smart et al., 2014).

Crustal eclogites distinguished by Stefano et al. (2009) are distinct macroscopically, as they have foliated texture, showing shape-preferred orientation of elongated garnets. The latter are more calcic, less magnesian, and are equilibrated with less jadeiitic omphacites (Kopylova et al., 1999a). Crustal origin has been assigned to the foliated eclogites based on REE patterns for bulk rock reconstructed from analysis for rare earth elements in fresh grains of clinopyroxene and garnet. Flat, unfractionated HREE and positive Eu anomaly in the pattern suggest mafic protoliths for these eclogites were formed by melting of the shallow mantle which did not contain garnet and crystallized at shallow depth in the plagioclase stability field (De Stefano et al., 2009). Crustal eclogites studied by Smart et al. (2014) demonstrate various bulk rock trace elements patterns (peaked, depleted, sloped), and the link between these and the texture and the mineralogy of the eclogite is unclear.

All studies of the Jericho eclogites agree that a subset of these rocks has a different origin. In De Stefano et al. (2009) opinion, this distinct variety of eclogites can be recognized by the massive texture. These eclogites that lack foliation comprise more magnesian minerals and show distinct diverse REE patterns in contrast to uniform patterns of the crustal eclogites with the foliated texture. The diverse and complex REE shapes imply more than one episode of rock formation, as does the petrography and mineral zoning, which provide evidence for several episodes of mantle metasomatism (De Stefano et al., 2009). Medium to strong HREE fractionation suggests a past coexistence with garnet now physically separated from the protolith, and the absence of Eu anomaly indicates that plagioclase was not involved in the rock formation. All these facts have interpreted as genesis of massive eclogites in a complex process that includes mantle, high-pressure *in-situ* melting in equilibrium with garnet and the subsequent melt extraction caused by metasomatising hydrous fluids (De Stefano et al., 2009). Because it’s difficult to untangle magmatic and metasomatic processes in formation of Jericho eclogites, their mantle origin implies a complex interplay of these processes.

In studies of Heaman et al. (2006) and Smart et al. (2014), this group of Jericho eclogites is distinguished based on the high-Mg mineral and bulk composition. Heaman et al. (2006) propose that they formed as ultramafic mantle cumulates or as metamorphosed olivine gabbros. The high-Mg eclogites have enriched LREEs and extreme Pb isotopic signatures (Fig. 5 and 7 of Smart et al., 2014). Smart et al. (2012) envisioned that the high-Mg eclogites formed as pyroxenite veins in the oceanic mantle, later re-melted and then subducted in the deeper mantle part of the slab. The model emphasizes the similarity of the eclogite bulk composition to pyroxenites found in orogenic massifs, the mantle affinity of the oxygen isotopes and the lack of any trace element signatures associated with plagioclase or seawater alteration. Thus, crustal, subduction-related origin of the high-Mg eclogites is postulated (Smart et al., 2014) or not excluded (Heaman et al., 2006), while an alternative point of view (De Stefano et al., 2009) advocates the mantle origin of these eclogites and ascribe the magnesian minerals with higher contents of some incompatible trace elements to metasomatic recrystallization of former less magnesian phases.

Studied eclogites of the Central Slave craton were collected from the Lac de Gras area, Ekati (Aulbach et al., 2011) and Diavik pipes (Schmidberger et al., 2007; Aulbach et al., 2007). Crustal origin in subducted slabs was suggested for all Diavik eclogites reported in Schmidberger et al., (2007), Diavik eclogites containing high-Mg and high-Ca garnets (Aulbach et al., 2007) and Ekati diamondiferous eclogites (Aulbach et al., 2011). This conclusion was based on flat, unfractionated REE patterns, subtle positive Eu anomalies, strong positive Sr and Pb anomalies, reconstructed bulk compositions resembling mafic cumulates (Schmidberger et al., 2007), and the presence of kyanite in the most Ca- and Al-rich eclogites (Aulbach et al., 2007). Low-Mg eclogites from Diavik, distinct from the above groups, may have formed in the hydrous arc mantle (Aulbach et al., 2007) rather than in the MOR mantle, like other crustal eclogites.

The eclogites from Northern and Central Slave craton yielded Proterozoic ages. The oldest of these are the 2.2 Ga Stacey-Kramers Pb model ages (Smart et al., 2014) and the 2.1 - 2.0 Ga Lu-Hf model ages of zircons (Schmidberger et al., 2005) for the Jericho crustal eclogites. These ages are similar to the oldest age for Diavik eclogites, 2.1 +/- 0.3 Ga based on the Lu-Hf whole rock isochron (Schmidberger et al., 2007). The ages were interpreted as the time of melt extraction from the depleted mantle in a mid-ocean ridge. Geochronology also established events of the eclogite formation around 1.8 - 1.7 Ga, coeval with subduction and orogeny. The first of these is the ~1.8 Ga mantle metasomatism and metamorphism that formed zircon and rutile in the Jericho eclogites of the crustal origin (Heaman et al., 2006). Secondly, clinopyroxene in Jericho and Muskox eclogites yield the 1.7 +/- 0.3 Ga secondary Pb isochron (Smart et al., 2014). Moreover, Diavik eclogites show the Nd and Hf addition at 1.7 Ga (Aulbach et al., 2007). These ages relate to eclogitization during east-dipping subduction of oceanic mafic volcanics at the western margin of the Slave craton during collision of the Hottah terrane and development of the Great Bear Magmatic arc (Heaman et al., 2006; Schmidberger et al., 2005; 2007; Aulbach et al., 2007; 2011) as part of the Wopmay orogeny at ~ 2.1 - 1.8 Ga (Cook, 2011). More precise estimate of eclogitisation of low-pressure oceanic crust is provided by the 1.86 ± 0.19 Ga Re-Os isochron on eclogitic sulphide inclusions in diamonds from Diavik (Aulbach et al. 2009). In addition, zircon-bearing crustal eclogite xenoliths from the Jericho kimberlite display a noteworthy abundance of Mesoproterozoic 1.3 Ga model Nd ages (Heaman et al., 2006), although no 1.3 Ga Pb model ages are observed (Smart et al., 2014). No ages are reported for mantle eclogites of the Northern Slave.

4. Analytical methods

A total of 76 Jericho eclogites (1 – 15 cm in diameter) and 33 Muskox eclogites (2 – 20 cm) were studied. Quantitative chemical analysis of minerals was conducted using a fully automated CAMECA SX-50 electron microprobe at the University of British Columbia in the Department of Earth, Ocean and Atmospheric Sciences. Analyses of all elements were completed using a beam current of 20 nA, acceleration voltage of 15 kV, and peak count time of 20 s. Cores and rims of garnet and clinopyroxene were analyzed for an average of four fresh grains for each sample, accessory and secondary minerals were also analyzed in select 15 thin sections (Electronic Supplementary Table 1).

Mössbauer analysis was performed on separates of garnet and clinopyroxene grains handpicked under a microscope from 0.5 to 2.0 mm size fractions of crushed and sieved rock material. The valence state of iron and its structural position in the minerals were determined using a SM-1201 Mössbauer spectrometer at the IPGG RAS (Saint-Petersburg, Russia) at room temperature in a constant acceleration mode over a velocity range of ±7 mm/s with a nominal 50 mCi ^{57}Co source in a Rh matrix. The spectrometer was calibrated relative to metallic iron at room temperature. The mineral grains were crushed in an agate capsule filled with acetone to avoid iron oxidation in contact with air, pressed in plastic discs and fixed on a special aluminum holder, ensuring an angle between gamma rays and absorber of 54.7°, to avoid asymmetry of the spectra due to preferred orientation of mineral grains. The density of the natural iron in the absorber was about 5 mg/cm^3. The spectra were approximated by a sum of Lorentzian lines using the MOSSFIT©software. The relative amounts of Fe^{2+} and Fe^{3+} and their site positions in the crystal lattice were determined from integral doublet intensities and hyperfine parameters. The quality of experimental spectra was assessed by background intensity and the quality of fitting by chi-square distribution. The fitting model for Grt included a single QS doublet for Fe^{2+} and Fe^{3+}. The relative peak widths and areas of the Fe^{2+} doublet, assigned to dodecahedral (distorted cube) site occupancy, were left unconstrained to account for spectra asymmetry (Amthauer et al., 1976). The doublet attributable to octahedrally coordinated Fe^{3+} was constrained to have components with equal widths and intensities. The Fe^{3+}/Fe_{tot} values obtained were corrected for different recoil-free fractions (Woodland and Ross,1994). The fitting model for Cpx included two symmetrical QS doublets for Fe^{2+} and one for Fe^{3+}. The hyperfine parameters and calculated proportions of Fe^{2+} and Fe^{3+} at different sites, calculated from HW and integral intensities of lines in QS doublets, are reported in Table 1. No additional lines were observed in any of the spectra, which confirms the absence of other mineral phases, including possible exsolutions. The absolute errors on the Fe^{3+}/Fe^{tot} ratios are about 0.015 for garnet and 0.030 for clinopyroxene.

5. Petrography of Northern Slave Eclogites

Eclogite xenoliths studied in this work were collected from exploration drill cores of the Jericho and Muskox kimberlite. Macroscopic and petrographic observations on mineralogy and texture were the basis for classification of the eclogites into two textural groups, massive or foliated.

The massive samples are composed of a bimineralic hypidioblastic aggregate of garnet (42 – 75 vol.%) and clinopyroxene (20 – 60 vol.%) (Fig 2A, F, G) with common accessory rutile (1-3%) (Fig. 2C) and biotite-phlogopite (1 vol.%) (Fig. 2B). Rare samples exhibit an unusual texture of round garnet blebs as inclusions within clinopyroxene grains. Garnet grains (3.4 mm average size at Jericho and 5.3 mm at Muskox) are round and anhedral containing few inclusions of opaques, clinopyroxene, apatite (Fig. 3C) and phlogopite laths. Kelyphitic rims are uncommon, and mainly occur where a garnet grain is in contact with carbonate alteration or veining. Anhedral clinopyroxene grains (3.9 mm average size at Jericho and 2.7 mm at Muskox) also contain few inclusions of garnet, opaques, biotite, and rarely rutile and other clinopyroxene grains. Twin lamellae occur along cleavage planes, and rare grains also contain thin lamellae of exsolved garnet, in common with other cratonic eclogites (Jerde et al., 1993a). Phlogopite grains (0.8 mm in size on average) are found as hypidioblastic laths as inclusions in clinopyroxene.

Rutile grains (2.4 mm in size on average) appear as rounded grains or clusters of hypidioblastic needles in Jericho samples and as xenoblastic rutile in Muskox xenoliths. Rutile may be mantled by opaques or ilmenite in the ~ 25 micron outer rim. Orthopyroxene and olivine grains are present in two Jericho samples. Sulfides are found as small round inclusions in clinopyroxene, garnet and rutile. Deformation is noticed in Jericho samples as undulatory extinction in clinopyroxene, but is less common in xenoliths from Muskox. Sample LGS035 Mx4 contains 5 vol. % prismatic or hexagonal idioblastic apatite (an average size of 0.4 mm), which is distributed evenly throughout the sample. The samples exhibit partial melting textures, i.e. "dusty" and turbid appearance of clinopyroxene near fractures and grain boundaries (Fig. 3A) due to multiple pores and small inclusions of crystallized melt. The prevalent daughter mineral that crystallizes from this melt is apatite as determined by the Raman analysis (ML Frezotti, pers. comm.). Partial melting is also evidenced by growth of fine euhedral grains of new clinopyroxene and zoned garnet on grain margins, analogous to the textures documented on Fig 4 of de Stefano et al., (2009).

The foliated eclogite is a bimineralic granoblastic aggregate of clinopyroxene (60-75 vol. %) and garnet (15-40 vol. %) with accessory rutile (1-7 vol. %), displaying a much higher volume content of clinopyroxene than the massive samples. All primary minerals are xenoblastic to hypidioblastic and show elongation in the same direction (Fig. 2B, D, E). Clinopyroxene (2.3 mm in size on average) and garnet (2 mm in size on average) grains are fractured and contain inclusions of rutile. Only clinopyroxene grains show little partial melting along grain boundaries and in fractures. Some deformation is manifested as undulatory extinction in clinopyroxene and the majority of phlogopite grains. Partial melting in the foliated eclogite is significantly less intense than in the massive eclogite (~5% vs. ~30%, respectively). Secondary melting of the eclogite results in the presence of a magmatic texture in some areas of the samples. These patches contain anhedral, curvilinear blebs of garnet included in clinopyroxene grains. Rutile grains (2 mm in size on average) occur as inclusions in garnet and clinopyroxene grains; larger grains are present between grains of clinopyroxene and/or garnet along the foliation.

Secondary alteration in massive and foliated xenoliths commonly occupies 4 – 12 vol. %; a few samples have 20 – 80 vol. % alteration (Fig. 2D, E). The main secondary minerals are serpentine, phlogopite, hornblende, carbonate, magnetite, unidentified opaques, and chlorite. This suite of minerals occurs in fractures on grain boundaries of garnet and clinopyroxene (Fig. 3 B, C, D), and more rare in veins. Green serpentine occurs on the outer edges of fractures and alteration patches, with yellow/colourless serpentine in the centre; both types form radiating fibers. Phlogopite generally forms hypidioblastic plates or interstitial xenoblastic grains. Fine opaque minerals and magnetite occur on the outer edges of alteration patches, or are associated with carbonate alteration and occur as inclusions in garnet and clinopyroxene grains. Carbonate is associated with phlogopite and opaques in all samples, occurring often in the center of veins or along fractures and grain boundaries, replacing and cutting through though primary minerals (Fig. 2B). Green amphibole in massive eclogites occurs in fractures, along grain boundaries, and in alteration patches of garnet grains and more rarely as hypidioblastic plates containing inclusions of spinel, opaques, phlogopite, and serpentine (Fig. 3C, D). The amphibole is rare in foliated eclogites and occurs only within garnet grains as anhedral plates in areas where the kimberlite has infiltrated the xenolith. Chlorite as either hypidioblastic plates or fibrous, radiating needles most often appears in intensely altered zones of the samples– usually between grains – and is associated with carbonate and phlogopite alteration. Occasionally, veins of carbonate with euhedral phlogopite in selvages cross-cut the rocks (Fig. 3B). Rare magnetite grains are present in thicker veins as euhedral inclusions in larger, poikilitic carbonate grains, implying the kimberlitic affinity of the vein material.

6. Mineral Chemistry

Analysed garnet compositions are typically dominated by almandine with lesser pyrope and grossular, $Almandine_{23\text{-}64}Pyrope_{21\text{-}46}Grossular_{13\text{-}35}$. Garnet in massive eclogites generally has a higher MgO content than that in the foliated eclogites; the latter has a wider range of CaO content displaced to lower values compared to massive samples (Fig. 4). There are positive correlations between MgO and Al_2O_3, as well as between TiO_2 (0.05 – 0.55 wt%) and Na_2O (0.05 – 0.14 wt%) in the garnet chemistry. All garnet rims, which experienced partial melting and recrystallization have a higher pyrope content than the primary garnet grains, i.e. $Pyrope_{50\text{-}73}Grossular_{11\text{-}27}Almandine_{15\text{-}22}$ (e. g. “secondary garnet” in samples 6-11, 55-4, 224.36; MOX24 206.9; MOX25 207 in EST1).

All clinopyroxene has an omphacitic composition with 20 – 80 mol. % diopside – hedenbergite, 80 – 20 mol. % jadeite and 0.1 – 0.5 wt% TiO_2. Omphacite in massive eclogites generally has a lower Na_2O and Al_2O_3 than the foliated eclogites (Fig. 5). Major element chemistry of clinopyroxene shows a positive correlation between Al_2O_3 and Na_2O (Fig. 5), and between MgO and CaO, which implies the residence of these elements in the jadeite and diospide end-members, respectively. Cr_2O_3 content correlates well with MgO and CaO. Analyses of recrystallized, secondary clinopyroxene grains (samples 20-7; 16-14; MOX7 53.9; MOX24 206.9; MOX25 207 in EST1) show an overall increase in diopside component at the expense of the jadeite component compared to the primary clinopyroxene.

Mossbauer estimates of ferric iron content yield 0.02 - 0.08 $Fe^{3+}/\Sigma Fe$ in garnet and 0.14 - 0.36 $Fe^{3+}/\Sigma Fe$ in clinopyroxene (Table 1). Ferric iron content in the clinopyroxene correlates with its total Fe content, whilst Fe^{3+} in garnet is crudely anticorrelated with its CaO content. The percentage of Fe^{3+} in garnet is lower than 10-25% assessed for Group A Udachnaya eclogites, but the Fe^{3+} in clinopyroxene covers the more narrow range of 20-22% $Fe^{3+}/\Sigma Fe$ in clinopyroxene documented for these eclogites (Sobolev et al., 1999).

Analyzed accessory minerals include orthopyroxene, olivine, apatite and opaques. Among Jericho samples, two massive eclogites with very magnesian minerals contain Fe-rich (Mg#=71) enstatite (sample 6-11 in EST 1) and low Ni forsterite Fo86 (sample JDF6NEcl in EST1). These samples are thus transitional to websterites. Apatite forming round inclusions in garnet and long primary-metasomatic prismatic grains are fluorapatites (2.2-3.6 wt% F, 0.7-2.1 wt.% Cl, 0.5-1.9 wt.% SrO). Rutile grains contain up to 3.4 wt.% Al_2O_3, up to 0.6 wt.% MgO, up to 2 wt.% Nb_2O_5 and up to 7.8 wt% FeO (e. g. samples 47-8, 47-2, MOX7 53.9; MOX25 207 in EST1). Iron content of rutile is controlled by the absence or presence of exsolved picroilmenite. Rutile from one massive Jericho eclogite (sample 55-4) is abnormally rich (3.5 – 4.1 wt%) in Nb_2O_5. Lamellae of ilmenite in rutile have highly variable compositions, with 12 - 19 wt% FeO total, and 0.8-3.1 wt% MgO. Picroilmenite rimming rutile has higher MgO content, 6.2 – 7.2 wt% MgO, and even more magnesian picroilmenite with 6.5 – 12.7 wt% MgO occurs as discrete grains in the eclogites. Pentlandite (0.8-1.3 wt% Co, 0.3 – 6.7 wt% Cu) forms small inclusions in clinopyroxene, pyrrhotite with 0. 6 – 9.8 wt% Ni occurs as small round inclusions in garnet and rutile; the pyrrhotite has rims of pentlandite with 0.1 – 3.7 wt% Co and of chalcopyrite with 1-2.1 wt% Ni. Millerite is also found among the sulfides.

Among secondary minerals present in veins, fractures, and patches replacing garnet and clinopyroxene, we analyzed phlogopite, amphibole, carbonates and magnetite. Phlogopite is 12 – 28 mol.% annite with 72 – 88 mol. % phlogopite end-member (e.g. samples MOX24 206.9; MOX25 207; MOX28 308.4; 47-8; 52-5 in EST1). There is no correlation between textural position of phlogopite in thin section and major element chemistry. The formula for phlogopite ranges from $(K_{0.8}Na_{0.1})(Mg_{1.9}Fe_{0.5}Ti_{0.1}Al_{0.1})(Si_{2.8}Al_{1.1})O_{10}(OH)_2$ to $(K_{0.9}Na_{0.1})(Mg_{2.2}Fe_{0.8}Ti_{0.2}Al_{0.3})(Si_{2.8}\ Al_{1.3})O_{10}(OH)_2$. Substitution between Al_2O_3 and SiO_2 is very limited and the amount of eastonite-siderophyllite is 0.1 to 0.3 mol. %. Amphibole shows wide variations in the composition (0.8 to 4.5 wt% Na_2O, 8-20% wt% CaO; 0-1.9 wt.% K_2O, 5-23% FeO; 0.1 – 4.2% TiO_2, 1.9 – 21.5 wt% Al_2O_3), classified as mostly tschermakite, transitioning to rare ferrotschermakite and edenite (Leake et al., 1997) (e. g. samples JDF6NEcl3, 52-5; JDF6NEcl; 47-8; MOX7 53.9 in EST1). Several different carbonate minerals are present in the eclogites analyzed (samples MOX7 53.9; MOX24 206.9; MOX25 207; MOX28 308.4 in EST1). These include calcite with variable FeO grading to siderite, with less common magnesite and dolomite. Composition of carbonate differs from sample to sample, for example specimen MOX28 308.4 only contains calcite, and magnesite is only found in eclogite MOX25 207. Magnetites are solid solution between magnetite, Cr-free spinel and ulvöspinel end-members, with compositions (sample MOX28 308.4 in EST1) $Fe^{2+}_{0.97}Fe^{3+}_{1.83}Ti_{0.07}Mg_{0.07}Mn_{0.04}Al_{0.02}O_4$ and $Fe^{2+}_{0.91}Fe^{3+}_{1.18}Al_{0.46}Mg_{0.26}Ti_{0.17}Mn_{0.01}O_4$.

7. Thermobarometry: The methodology

Mineral compositions of clinopyroxene and garnet were used to infer the temperature and pressure of the eclogite formation. Distribution of Fe and Mg between omphacite and garnet was calibrated many times producing multiple clinopyroxene - garnet thermometers. We calculated temperatures using the most recent calibration of Nakamura (2009), which accounts for ferric iron and can be used accurately at 800 – 1800^o and 15 – 75 kbar with accuracy ± 74^o. The

Nakamura (2009) thermometer improves on the old Ellis and Green (1979) formulation as it allegedly eliminates overestimation of temperature below 1000^{o}C by 20 – 100^{o}. Indeed, as seen on the histograms for different compositional types of eclogites (Fig. 6), Nakamura (2009) temperatures yield modes that are 50^{o} lower compared with Ellis and Green (1979) for similar sample groups.

Recently calibrated barometer for eclogites (Beyer et al., 2015) allows computing pressure for samples with a large amount of tetrahedrally coordinated Al in omphacites (Si cpfu < 1.875). To assess if the barometer can be employed for our study we applied it to the subset of diamondiferous Slave eclogites combining the pressures with the Nakamura temperatures (Fig. 7). Eleven of 21 eclogites plot too shallow, outside of the diamond stability field, although the upper parts of the pressure uncertainty (+/-6 kb) extend into the diamond field. The errors of the barometer are higher for samples with lower tetrahedral Al; for these high-Si omphacites pressures are overestimated and error reaches 12 rel.%. The beyer-Nakamura pressure-temperature estimates for Jericho diamondiferous eclogites define the widely varying heat flow, from 33 in the asthenophere to 46 mW/m^2 in the lithosphere, rather than falling into the 40 mW/m^2 steady state geotherms of the Northern and Central Slave (Fig. 7).

We chose not to employ the Beyer et al. (2015) barometry for several reasons. Firstly, it makes impossible one of the study goals, the comparison between eclogites of the Northern and Central Slave. Measured concentrations of Si in clinopyroxene are extremely sensitive to the choice of reference standards for microprobe analyses and vary between analytical laboratories. We found that Si in all analyses of omphacites carried out in the GEMOC National Key Center (Pearson et al., 1999; Aulbach et al., 2007; 2011) are consistently higher than those reported from elsewhere. For example, out of 33 eclogites of the A154S pipe (Aulbach et al., 2007), only 6 can be used for barometry, while others contain Si> 4.000 cpfu (60%) and 4.000 < Si < 1.985 (24%). Since the data for the Central Slave are dominated by these samples, not amenable to the Beyer barometry, the Central Slave dataset would be diminished to negligible numbers. Furthermore, if we accept Beyer et al. (2015) pressure estimates as accurate, we should postulate the thermal disequilibrium between intercalated eclogites and peridotites of the same mantle segment, a lower geotherm in the asthenosphere than for the lithosphere, and derivation of a considerable part of eclogites from the cold asthenosphere (Fig. 7). All these heretical conclusions contradict the established view of the mantle, and changing the mantle paradigm would require a lot of confidence in the new barometric calibration, which we currently do not have.

Without the eclogite barometry, we placed eclogites at depth by intersecting the Nakamura (2009) P-T solution line with the geotherm constrained for peridotites using Brey and Köhler (1990) thermobarometry as exemplified by sample EA005 on Fig. 7. The peridotitic P-T array (Kopylova et al., 1999b) uses a two-pyroxene thermometer and a garnet-orthopyroxene barometer. This Brey and Köhler (1990) thermobarometric combination is widely employed for mantle peridotites and pyroxenites (e.g. Bell et al., 2003; Kopylova and Caro, 2004; Menzies et al., 2004) and was proven to satisfy available petrological constraints for Jericho xenoliths i.e. placing diamondiferous eclogites in the diamond stability field and spinel-garnet peridotites at the spinel-garnet transition line (Kopylova et. al. 1999b). The projection of eclogitic univariant P-T lines onto a peridotitic geotherm is based on the assumption that the eclogites are thermally equilibrated with the peridotites, which is expected for texturally equilibrated metamorphic rocks residing for more than 1 Ga together at T= 800- 1300°C. The internal consistency of the Brey and Köhler (1990) thermobarometry with the Ellis and Green (1979) temperatures for eclogites was checked and proven to give correct results for diamondiferous eclogites (Kopylova et al., 1999a).

Since eclogite thermometers rely on the Fe^{2+}-Mg exchange between omphacite and garnet, the computed equilibrium temperatures would be most significantly affected by either neglecting Fe^{3+} or using incorrect values. Therefore we calculated Nakamura (2009) temperatures that account for Fe^{3+} in both clinopyroxene and garnet using the Mossbauer values of $Fe^{3+}/\Sigma Fe$ for samples analyzed for Fe^{3+}. The temperatures turned out to be 50-165°C lower than the temperatures computed without correction for Fe^{3+} (Table 1). This would translate to pressures lower by 5-16 kb (17-52 km in depth). If the $Fe^{3+}/\Sigma Fe$ values were extrapolated to all analyzed eclogitic minerals (taking into account correlations of Fe^{3+} with total Fe and Ca) and applied to all Northern Slave eclogites, the resulting temperatures would be unreasonably low. For example, diamondiferous Jericho samples (De Stefano et al., 2009; Smart et al., 2012) plot at 900-970°C and 39-47 kb if the Nakamura (2009) P-T lines are projected onto the Jericho Brey and Köhler (1990) geotherm. This depth position is on the shallow threshold of the diamond stability field. Lowering the temperatures for 50-165°C by accounting for Fe^{3+} would place diamondiferous eclogites outside of the diamond stability field, at T=740 - 810°C, P = 32-35 kb. Because of this, we did not use the Fe^{3+} correction when calculating temperatures for the Slave eclogites. Application of the chosen thermobarometric algorithm to diamondiferous eclogites of Diavik (Schmidberger et al., 2005) and Ekati (Aulbach et al., 2011) prove its robustness by placing 14 out of 15 samples in the diamond stability field at P=55-65 kb and T=1150-1350oC.

8. Thermobarometry: The results

Temperatures for Jericho eclogites were computed for the studied samples (EST1); additionally, literature analyses (Heaman et al. 2006, Smart et al. 2009, Kopylova et al. 1999a, and Kopylova et al. 2004) have been included in the calculations and the following discussion. These eclogites, at the estimated equilibration pressure of 50 kbar, record temperatures from 850 to 1250°C (Fig. 6). Divided by mineral chemistry into Groups A, B and C and projected onto the Jericho peridotite geotherm, Jericho eclogites plot at 100-240 km (Fig. 8). Temperatures and pressures of geotherm intersections for 59 massive xenoliths range from 730 to 1305°C and from 30 to 80 kbar (Fig. 9A). Sixty one foliated eclogite xenoliths are equilibrated at 775 to 1230 °C and from 35 to 73 kbar, mostly in the diamond stability field (Fig. 9A).

Eclogite xenoliths from the Muskox kimberlite at P of 50 kbar record temperatures from 800 to 1200°C. Groups A, B and C eclogites projected onto the Jericho peridotite geotherm yield depths of 80-230 km (Fig. 8). Comparison with the Jericho eclogites demonstrates the general similarity of the Groups A and B depth distribution, but the absence of shallow Group C eclogites sourced from depths above 140 km at Muskox. This matches well with the wider range of garnet and clinopyroxene compositions from Group C Jericho eclogites compared with the Muskox samples. The extremely jadeitic clinopyroxenes and grossular-rich garnets of more shallow Group C eclogites are missing at Muskox (Fig. 4, 5). Temperatures and pressures of intersections with the geotherm for 17 massive eclogites range from 670 to 1290 °C and from 25 to 78 kbar. Foliated eclogites (N=11) range from 870 to 1100°C and from 43 to 54 kbar. The foliated eclogites span a narrower range of pressures and temperatures than the massive eclogites (Fig. 9B) and plot fully in the diamond stability field.

For both Jericho and Muskox pipes, foliated eclogites demonstrate a tighter unimodal depth distribution than massive eclogites. Because of this pattern, and because the Muskox dataset is not large enough compared to the statistically significant Jericho and Central Slave thermobarometric data, we combined the Jericho and Muskox eclogites and in further graphs plotted these as "Northern Slave" eclogites.

As the goal of the study was to get a consistent, directly comparable set of equilibrium temperatures and pressures for all eclogites of the Slave craton, we also used the Nakamura (2009) thermometer not corrected for Fe^{3+} in clinopyroxene and garnet for eclogite xenoliths of the Central Slave reported in the literature. The Central Slave eclogites (a total of 91), at pressure of 50 kbar, record temperatures from 700 to 1350^{o}C. These temperatures were projected onto the Central Slave geotherm from Menzies et al. (2004) constrained with the Brey and Köhler (1990) thermobarometry to yield the depth distribution (Fig. 8). Divided by mineral chemistry into Groups A, B and C, the Central Slave eclogites plot at 90-230 km (Fig. 8). All the eclogite groups show a bimodal depth distribution, with the shallow mode at 130-140 km and the deeper modes slightly shifted in depth between the groups. A thorough petrographic work is needed to correlate the depth modes with the history of the rock formation.

8. Discussion

8.1 Depth distribution of crustal eclogites in the Slave mantle

The combined internally consistent, statistically significant dataset enables comparison between Northern and Central Slave eclogites of crustal origin. We assumed textural and trace element criteria for the crustal origin, i.e. considered "crustal" all Jericho and Muskox eclogites with the foliated texture. For the Central Slave, we plotted as "crustal" all eclogites interpreted in the respective papers as metamorphosed subducted slabs (Schmidberger et al., 2007; Aulbach et al., 2007; 2011). The comparison between crustal eclogites for Jericho, Muskox and Central Slave thus defined is shown on Fig. 9. The 150 km NW - SE mantle cross-section from Northern to Central Slave demonstrates distribution of crustal eclogites in the Slave mantle, with equal vertical and horizontal scales (Fig. 10A). The Central Slave eclogites of the crustal, subduction origin occur at 120-210 km, deeper than the Northern Slave crustal eclogites (110-170 km). This conclusion would still stand if we add high-Mg Jericho eclogites to crustal eclogites of the Northern Slave. These eclogites of the controversial origin were interpreted either as subduction-related and formed in the oceanic mantle (Smart et al., 2012) or metasomatically produced in the cratonic mantle (De Stefano et al., 2009). Because both populations of eclogites record the same geochemical and formation history, with the 2.1 - 2 Ga original mantle melting and the ~1.8 Ga subduction and metamorphism, the eclogites of the Northern and Central Slave may have the identical origin and represent the same extended geological body. To constrain a possible morphology of this body and to extrapolate the eclogite distribution between the north and the center of the craton we turn to geophysics.

Geometrical information at depth on layers and mantle domains within the Slave mantle is provided by compilation of datasets on seismic discontinuities, obtained through P-wave and surface-wave velocity models, Ps received functions and conductivity models (Snyder et al., 2014). The compilation recognized that the Slave is built from several laterally-discontinuous lithospheric domains that abut each other along wedged steep faults (Fig. 11). Even though their direct geophysical imaging is not possible, the near-vertical discontinuities can be inferred from 1) offsets in horizontal discontinuities; 2) lateral gradient in surface wave velocity at 50-150 km 3) polarity flips. Such domain boundaries are mapped around the Slave craton, beneath MacKay Lake, 25 km south of Diavik, and beneath Nicholas Bay of Aylmer Lake, where a schematic cross-section of Fig. 11 shows juxtaposition of distinct terranes. A steep suture boundary beneath the MacKay Lake in the central Slave craton (Fig. 11), may separate the Proterozoic slab dipping to the east from a Late Archean subducted slab with a opposite dip direction (Fig. 15 of Snyder, 2008). This would explain why the layered anisotropic structure the southeastern Slave craton (east of the MCKN station on Fig. 1) is distinctly different, demonstrating more numerous, weaker impulses, with the opposite polarity to that observed farther north (Snyder, 2008).

No domain boundaries are mapped geophysically between the Jericho and Ekati-Diavik, suggesting the continuity of the mantle rich in crustal eclogites. Proterozoic ages of most Slave eclogites (Heaman et al., 2006, Smart et al., 2014, Aulbach et al., 2007, Schmidberger et al., 2005; 2007; Heaman and Pearson, 2010) and many mantle peridotites, especially in the NW part of the craton (Heaman and Pearson, 2010; Pearson et al., 2015) suggest that the localization of crustal eclogites may reflect the geometry of a single lithospheric relic slab formed by Proterozoic subduction. This slab may be a continuation of the Proterozoic oceanic slab beneath the southwestern part of the Slave mantle (Fig. 10B) mapped by

- Dipping discontinuity in the reflection studies that corresponds to the frozen Proterozoic subduction. The mantle discontinuity to the west of the Slave craton extends to Proterozoic crustal rocks on the surface (Cook et al., 1995; Cook and Erdmer, 2005).
- Teleseismic studies in the SW Slave craton (Bostock, 1998).
- Fine-scale mantle anisotropy in the SW Slave (Bostock, 1998), North and Central Slave as far east as the McKay Seismic Station (Fig. 1; Snyder et al., 2004, Snyder, 2008) characteristic for the subducted oceanic lithosphere (Mercier et al., 2008).

Thicknesses of the petrologically-observed eclogite-rich areas are 60-90 km, much thicker than the oceanic crust, so we should assume tectonic imbrication of the slab and possible plastic thickening and dispersion *in situ*. The sharp shallow onset of the eclogites and the gradual disappearance of eclogites at the deeper end of the interval speaks of the preferential sinking of eclogites rather than an even dispersal in all directions. The sinking of denser eclogite (Kopylova et al., 2004) through the lighter peridotitic keel was invoked as one of root purging processes (Pearson and Wittig, 2008). The dispersal of former oceanic crust in the mantle in wider interval of pressures is a natural consequence of mixing in with peridotite. Since thermobarometric observations on Slave mantle xenolithd (Kopylova et al., 1999b; Newton et al., 2015) requires peridotites and eclogites be sourced from the same depth, the eclogite-only oceanic crust should intercalate with peridotite. As a consequence, eclogite is diluted with 96-99% peridotite (Schulze, 1986; Russell et al., 2001' Mclean et al., 2007) and distributed over a wider depth interval. Our data show that despite this, the general slab orientation and geometry may be somewhat maintained.

The bimodal depth distribution of eclogites beneath Central Slave (Fig. 10A, B) may correspond to the separation of the Paleoproterozoic upper mantle into a 1.92 - 1.88 Ga slab subducted during the Wopmay orogeny and the 1.90 - 1.88 Ga slab underthrust below as a result of the subsequent Great Bear orogeny (Cook and Erdmer, 2005; Helmsteadt, 2009). It would also be tempting to correlate the bimodal depth distribution of the Central Slave eclogites with the presence of two overlapping layers defined by teleseismic discontinuities with the different dipping directions (Snyder, 2008) and with the position of the Mid-lithosphere discontinuity (Fig. 11)

Our interpretation of the crustal eclogite distribution as reflecting the subducted Proterozoic slab agrees with the expected angles of ancient subduction. The roof of the slab as constrained petrologically dips to the southeast at apparent dip 12^{o}, whilst the base of the slab also dips to the southeast, but at a steeper angle, ~17^{o} (Fig. 10A). One can access the true dip of the slab at 23^{o}-27^{o}, based on the apparent dip and the orientation of the NW-SE cross-section line with respect to N-S orientation of the Wopmay and the Great Bear subduction zone strikes to the west of the Slave craton (Fig. 1). The calculated 23-27^{o} true dip of the Proterozoic slabs resembles shallow Archean subduction, for example, the 20-25^{o} angle of the 2.69 Ga Archean Abitibi slab thrusting 30 km into the mantle beneath the northern Opatica terrane (Calvert et al., 2005). These slab geometries are dissimilar to steep dips of modern (0-90 Ma) subduction (>35^{o}, Lallemand et al., 2005).

Our interpretation of some eclogites from the deeper part of the Slave lithosphere as the metamorphosed subducted slab dictates the presence of oceanic, depleted peridotites from the deeper mantle part of the lithospheric plate at depths below 110 km. In agreement with this, Proterozoic Re-Os model ages are recorded fro the Northern and Central Slave mantle peridotites alike (Heaman and Pearson, 2010). The ages become more abundant in the NW part of the craton (Pearson et al., 2015) and in the deeper parts of the craton (Irvine et al., 2012). Moreover, formation of some Northern Slave eclogites in the mantle part of the subducted oceanic slab was argued by mantle d^{18}O values and trace element patterns (Smart et al., 2012).

8.2 Geophysical expression of mantle eclogites

Even though eclogites are much denser than surrounding peridotites and support faster seismic velocities at depths below 100 km (Kopylova et al., 2004), eclogites comprise less than 4 vol.% of the cratonic mantle (Schulze, 1986; Russell et al., 2001; McLean et al., 2007) and may not necessarily be visible in geophysical surveys. A comparison of depths of eclogite localization in the Slave mantle with seismic discontinuities supports this.

Two discontinuities in the mantle of the Northern and Central Slave were mapped by several seismic surveys, the mid-lithosphere discontinuity (MLD), and a local Lac de Gras discontinuity (Snyder et al., 2014). MLD is a near horizontal boundary at 140-160 km (Fig. 11), typical of Precambrian shields in general (Yuan et al., 2011). Its detection mainly on the transverse component suggests no change in the bulk rock property is associated with the discontinuity. Indeed, depths of 140-155 km are in the middle of the eclogite distribution and equal proportions of eclogites are expected above and below MLD (Fig. 11). Another discontinuity is seen only below Central Slave, where it dips from 85 to 110 km to the southeast (Fig. 11), i.e. at depths shallower than those populated by eclogites. It would be tempting to correlate the gap in the bimodal depth distribution of the Central Slave eclogites (Fig. 10A) with the mid-lithosphere discontinuity (Fig. 11) and the presence of two overlapping layers defined by teleseismic discontinuities with the different dipping directions (Snyder, 2008). These two layers were interpreted as separation of the Paleoproterozoic upper mantle into a 1.92 - 1.88 Ga slab subducted during the Wopmay orogeny and the 1.90 - 1.88 Ga slab underthrust below as a result of the subsequent Great Bear orogeny (Fig. 10, Cook and Erdmer, 2005; Helmsteadt, 2009).

The comparison of petrological and seismic data suggest that neither the upper, nor the lower limit of the eclogite-enriched mantle is expressed as a discontinuity. The base of the eclogite-bearing slab coincides with the petrological lithosphere-asthenosphere boundary, which is geophysically invisible in the Slave and globally (Snyder et al., 2014). The slab lies below the complexly-shaped Slave mantle with enhanced electric conductivity (Jones et al., 2001; Snyder et al., 2014).

A correlation between anisotropy and the presence of eclogites may be more feasible. Eclogites are less anisotropic than peridotites (e.g. Bascou et al., 2011), as nearly half of the rock volume is made of isotropic garnet. Experimentally determined anisotropy of massive Jericho eclogites yielded 0.2 – 2.4 % for Vp and 0.4 – 1.0% for Vs; the values for foliated eclogites are higher, 2.0 - 8.1% and 0.4 – 3.8% (Kopylova et al., 2004). Anisotropy of peridotite is stronger, 2.5-10.2%

for Vp and 2.7 – 8% for Vs (Baptiste and Tommasi, 2014), representing lattice-preferred orientation of olivine (Fouch and Rondenay, 2006), with no contrast in the anisotropy between the lithospheric coarse and the asthenospheric sheared peridotites (Ben-Ismail et al., 2001; Baptiste and Tommasi, 2014).

Depth intervals containing eclogites correspond to depths with moderate and weak seismic azimuthal anisotropy (100-200 km) detected on the Canadian Shield using the range of all techniques currently available to image seismic anisotropy with passive source seismic data (Fouch and Rondenay, 2006; Fig. 11). The strongly anisotropic mantle is mainly restricted to shallow levels, above 100 km, where eclogites are absent. The weaker anisotropy with the increasing depth from 160 to 200 km (Fig. 11) correlates with an increased proportion of young massive magmatic garnet websterites with depth, as mapped below Jericho (Kopylova et al., 1999b) and Muskox (Newton et al., 2015). However, this generalized and low-resolution model of the anisotropy of the Canadian Shield has yet to be reconciled with a better resolved analysis of the Slave mantle anisotropy (Snyder and Bruneton, 2007; Snyder et al., 2008). The unambiguous depth assignment of anisotropy is hampered by the fact that discontinuities mapped by conversions of P-waves into S-waves may be caused by changes of either velocity, density or anisotropy. Furthermore, if a discontinuity is modelled by a change in anisotropy, it could mark either the top or bottom of the anisotropic layer (Snyder et al., 2004). The new synthesis of the Slave geophysical data that includes the SKS –splitting parameters confirms that the weakening of seismic anisotropy at ~ 150 km coincides with MLD (Snyder et al., 2014). Seismic analysis applied to stations in the Central Slave discovered the observed patterns of phase reversal and impulse arrival times strongly indicative of 1–4% anisotropy in layers dipping at 22° to the southeast (Snyder et al., 2008), i.e. matching the expected geometry and the anisotropy of eclogitic slab. Overall, the fine-scale, anisotropic mantle layering expressed as +/- 5% variation in shear velocity observed under western and central Slave may be a generic hallmark of shallow subduction (Mercier et al., 2008).

8.3 Eclogites in the peridotitic mantle

Spatial relationships between eclogitic and peridotitic mantle provide insights into mantle processes in the cratonic roots. The deep limit of the eclogite distribution coincides with the base of the Slave depleted lithosphere (Fig. 11). Very few eclogite samples are sourced from below the base, and we think this is not a coincidence, but a robust observation that calls for an explanation.

The cross-section of Fig. 11 draws the base of the depleted lithosphere as the lithosphere-asthenosphere boundary. Several criteria have been used in the past to define petrological lithosphere. It can be construed as the ancient peridotitic isotopic reservoir requiring long-term isolation from the convecting asthenospheric mantle (e.g. Pearson and Nowell, 2002). It can also be defined as the chemically depleted layer (e.g. Eaton et al., 2009), which is expressed below cratons in low Ti, Ca and Fe contents of all mantle phases (e.g. Boyd and Nixon, 1979; Boyd and Gurney, 1986), trace element chemistry of garnet, Mg-number of olivine (e.g. Griffin et al., 1999; 2004) and multiple other indicators of melt depletion. The depth where peridotites acquire the fertile mineral chemistry match several other pronounced changes in mantle peridotites, i.e. the shallow limit of occurrence of young, unequilibrated deformed texture (Boyd and Gurney, 1986, Kopylova and Caro, 2004; Eaton et al., 2009), the depth where the steady-state geotherm becomes perturbed (Kopylova et al., 1999b; Bell et al., 2003; Eaton et al., 2009; Janney et al., 2010) and the depth where diamonds disappear from peridotites (so-called “Diamond Window” , Griffin et al., 1999). This significant P-T boundary was interpreted as the lithosphere-asthenosphere boundary (e.g. Boyd and Gurney 1986; Kopylova and Caro, 2004; Heaman and Pearson, 2010), as the base of “depleted lithosphere” (Griffin et al., 1999; 2004) or as the base of the “thermal transition layer”, i.e. the lithospheric mantle modified by asthenospheric melts shortly prior to the kimberlite eruption (e.g. Eaton et al., 2009). The interpretations are not entirely mutually exclusive, as one should expect the metasomatism be especially strong immediately above the asthenosphere, and the restriction of pre-kimberlitic metasomatism and recrystallization to the mantle below the boundary may just articulate the hidden distinct character of the mantle there. However one calls this significant boundary, it is expressed in many cratonic materials, such as macrocrysts and peridotite xenoliths, and in many independent petrological characteristics of these materials.

An alternative approach to defining the petrological lithosphere is less grounded in empirical data and relies more on thermal modeling. It defines lithosphere as the “thermal boundary layer” with the conductive heat transfer (e.g. Rudnick et al., 1999; Mather et al., 2011). The approach constrains the steady-state conductive geotherm based on empirical pressures and temperatures of cratonic peridotite xenoliths, but ignores the important P-T barrier where peridotites cease to be chemically depleted and thermally perturbed (Rudnick and Nyblade 1999; Mather et al., 2011). Instead, the modeling seeks the intersection of the steady-state geotherm that best fits the observed P-T array with the theoretical adiabate. The latter varies by almost 100^o, from 1315^{o}C as assumed in Mather et al., (2011), to the commonly accepted 1400^{o}C (e.g. Mosenfelder et al., 2009). Moreover, some empirical P-Ts recorded in high-T cratonic peridotites exceed the theoretical adiabates (Eaton et al., 2009). The lithosphere thickness in this modeling depends not only on the assumption on the temperature of the adiabate, but also on whether high-T peridotites are assumed to be on the steady-state geotherm (Rudnick and Nyblade 1999) or not (Mather et al., 2011).

On Fig. 11 and in Kopylova and Caro (2004) we mapped the "depleted lithosphere" thickness using the most direct approach rooted in empirical xenolith data. The asthenospheric roof is mapped by thermobarometry of the sheared high-T peridotitic xenoliths in various kimberlites of the Slave craton (Kopylova and Caro, 2004; Menzies et al., 2004) and is seen as the area of thermal disturbance and metasomatism. The base of the lithosphere dips from 160 km in Northern Slave (Kopylova et al., 1999b) to at least 210 km beneath the Central Slave and at least 250 in the SE Slave. The latter two depths are constrained by the absence of high-T peridotites from depths above 210 km (62 kb, Menzies et al., 2004) and 250 km (76 kb, Kopylova and Caro, 2004) from Ekati and Gahcho Kue pipes, respectively. The spatial coincidence of the depleted lithosphere base with the depth of eclogite disappearance from the mantle (Fig. 11) cannot be an artifact of the thermobarometric method used to infer the depth of the eclogite. Pressures for these samples can only be overestimated rather than calculated as artificially low, as our thermobarometric algorithm seeks an intersection of the undisturbed, steady-state peridotitic geotherm with the eclogitic thermometry.

The spatial coincidence of the inferred oceanic slab and the deep part of the lithosphere may mean their causal link. Firstly, the cratonic root may have initially been built around the recycled and imbricated oceanic lithosphere (e.g. Pearson and Wittig, 2008), inheriting its architecture.

The initial Slave cratonization may have occurred through subcretion of one or two slabs during NW- or SE-vergent underthrusting 2635 – 2615 Ma (Davis et al., 2003; Snyder, 2008; Helmsteadt, 2009; Snyder et al., 2015). The Archean and later Proterozoic tectonic underplating may have armored the base of the Archean lithosphere above, thus shielding and preserving the colder mantle from the asthenospheric invasion from below (Bostock, 1998). The lithosphere could be eroded, and penetration of hot asthenospheric metasomatizing melts is the first step in making the lithosphere weaker and denser (Lee et al., 2005 and references therein). Indeed, metasomatism is more pronounced in the deeper part of the Slave lithosphere, as seen, for example, in the reported restriction of fluid metasomatism in the C. Slave mantle to depths below 120 km evident in the Sm-Nd /Lu-Hf characteristics of minerals in Central Slave peridotites (Aulbach et al., 2013). Proterozoic Re-Os isotope data for Slave peridotite xenoliths and their increased significance towards the northern margins of the Slave (Pearson et al., 2015) suggest that the Proterozoic subducted mantle lithosphere may be a more significant component of the Archean roots and Proterozoic underthrusting aided in stabilization for Archean cratons (Helmsteadt, 2009).

9 Conclusions

1. Crustal eclogites are localized at depths 100-200 km below the Slave craton, possibly reflecting the original geometry of the subducted Proterozoic slab.
2. Eclogites may be geophysically invisible
3. The deep limit of the eclogite distribution coincides with the base of the Slave depleted lithosphere
4. Three-D architecture of buried subducted slabs underthrust under older peridotitic mantle may control the geometry of the cratonic root.

Acknowledgements

The study was possible due to a generous donation of samples from Canamera Geological Ltd. The research was supported by an NSERC Discovery Grant to MGK.

References

Amthauer, G., Annersten, H., Hafner, S. S., 1976. The Mössbauer spectrum of ^{57}Fe in silicate garnets. Z Kristallogr 143, 14–55.

Aulbach, S., Pearson, N. J., O'Reilly, S. Y., Doyle, B. J., 2007. Origins of xenolithic eclogites and pyroxenites from the central Slave Craton, Canada. J.of Petrology 48, 1843-1873.

Aulbach, S., Shirey, S. B., Stachel, T., Creighton, S., Muehlenbachs, K., Harris, J.V., 2009a. Diamond formation episodes at the southern margin of the Kaapvaal Craton: Re-Os systematics of sulfide inclusions from the Jagersfontein Mine. Contr. Miner. Petrol. 157, 4, 525-540.

Aulbach, S., Stachel, T., Creaser, R. A., Heaman, S.V., Shirey, S. B., Muehlenbachs, K., Eichenberg, D., Harris, J.V., 2009b. Sulphide survival and diamond genesis during formation and evolution of Archaean subcontinental lithosphere: A comparison between the Slave and Kaapvaal cratons. Proceedings of the 9th International Kimberlite Conference. Lithos 112S, 747–757.

Aulbach, S., Stachel, T., Heaman, L. M., Carlson, J. A., 2011. Microxenoliths from the Slave craton: Archives of diamond formation along fluid conduits. Lithos 126, 419-434.

Aulbach, S., 2012. Craton nucleation and formation of thick lithospheric roots. Lithos 149, 16–30.

Aulbach, S., Griffin, W. L., Pearson, N. J., O'Reilly, S. Y., 2013. Nature and timing of metasomatism in the stratified mantle lithosphere beneath the central Slave craton (Canada), Chem. Geol., 352, 153-169.

Baptiste V, Tommasi A., 2013. Petrophysical constraints on the seismic properties of the Kaapvaal craton mantle root. Solid Earth 5 (1), 45-63.

Barth M.G., Rudnick, R. L., Horn, I., McDonough, W. F., Spicuzza, M. J., Valley, J. W., Haggerty, S. E., 2001. Geochemistry of xenolithic eclogites from West Africa, Part I: A link between low MgO eclogites and Archean crust formation. Geoch. Cosmoch. Acta 65 (9), 1499-1527.

Barth M.G., Rudnick, R. L., Horn, I., McDonough, W. F., Spicuzza, M. J., Valley, J. W., Haggerty, S. E., 2002, Geochemistry of xenolithic eclogites from West Africa, part 2: Origins of the high MgO eclogites. Geoch. Cosmoch. Acta 66 (24), 4325-4345.

Bascou, J., Doucet, L.S., Saumet, S. et al. 2011. Seismic velocities, anisotropy and deformation in Siberian cratonic mantle: EBSD data on xenoliths from the Udachnaya kimberlite. Earth and Planetary Science Letters, 304, 1-2, 71-84

Beard, B.L., Fraracci, K.N., Clayton, R.A., Mayeda, T.K., Snyder, G.A., Sobolev, N.V., Taylor, L.A., 1996. Petrography and geochemistry of eclogites from the Mir kimberlite, Yakutia, Russia. Contr. Miner. Petrol. 125 (4), 293–310.

Bell, D. R., Schmitz, M. D., Janney, P. E., 2003. Mesozoic thermal evolution of the southern African mantle lithosphere. Lithos, 71, 273-287

Ben-Ismail, W., Barruol, G., Mainprice, D., 2001. The Kaapvaal craton seismic anisotropy: petrophysical analyses of upper mantle kimberlite nodules. Geoph. Res. Lett. 28 (13), 2497-2500

Beyer, C., Frost, D. J., Miyajima, N., 2015, Experimental calibration of a garnet-clinopyroxene geobarometer for mantle eclogites. Contrib. Miner. Petrol., 169. 10.1007/s00410-015-1113-z

Bleeker, W., Hall, B., 2007. The Slave Craton: geology and metallogenic evolution. In: Goodfellow, W. D. (ed.) Mineral Deposits of Canada: A Synthesis of Major Deposit-Types, District Metallogeny, the Evolution of Geological Provinces, and Exploration Methods. GAC Mineral Deposits Division, Special Publication 5, 849-879.

Bostock, M. G., 1998. Mantle stratigraphy and evolutionof the Slave province. J. Geoph. Res. 103, B9, 21,183 - 21,200

Boyd, F. R. and Nixon, P. H., 1979. Garnet lherzolite xenoliths from the kimberlites of East Griqualand, South Africa. Carnegie Inst. Washington tearbook, 78, 488-492

Boyd, F. R., and Gurney, J. J., 1986. Diamonds and the African lithosphere. Science, 232, 472-477

Brey, G. P., Köhler, T., 1990. Geothermobarometry in four-phase lherzolites II. New thermobarometers, and practical assessment of existing thermobarometers. J Petrol 31, 1353–1378.

Calvert, A. J., Sawyer, E. W., Davis, W. J., Ludden, J. N., 1995. Archean subduction inferred from seismic images of a mantle suture in the superior province. Nature 375 (6533), 670-674.

Coleman, R. G., Lee, E. D., Beatty, L. B., Brannock, W. W. , 1965. Eclogites and eclogites: their differences and similarities. Geol. Soc. of America Bull. 76, 483-508.

Cook, F.A., van der Velden, A. J., Hall, K. W., Roberts, B. J., 1999. Frozen subduction in Canada's Northwest Territories: Lithoprobe deep lithospheric reflection profiling of the western Canadian Shield. Tectonics 18, 1, 1-24.

Cook, F.A., Erdmer, P., 2005. A 1800 km cross-section of the lithosphere through the northwestern North American plate: lessons from 4.0 billion years of Earth’s history. Can. J. Earth Sci. 42, 1295-1311.

Cook, F. A., 2011. Multiple arc development in the Paleoproterozoic Wopmay Orogen, northwestern Canada. In: Brown, D., Ryan, P. D. (eds) Arc-Continent Collision, Frontiers in Earth Sciences. Springer: Berlin, 403-428.

Davis, W. J., A. G. Jones, W. Bleeker, and H. Grutter (2003), Lithospheric development in the Slave cra ton: A linked crustal and mantle perspective, Lithos, 71, 575 – 589, doi:10.1016/S0024-4937(03)00131-2.

De Stefano, A., Kopylova, M. G., Cartigny, P., Afanasiev, V., 2009. Diamonds and eclogites of the Jericho kimberlite (Northern Canada). Contr. Miner. Petrol. 158, 295-315.

Eaton, DW; Darbyshire, F; Evans, RL; Grutter, H; Jones, AG; Yuan, XH, 2009. The elusive lithosphere-asthenosphere boundary (LAB) beneath cratons. Lithos, 109, 1-2: 1-22

Ellis, D. J., Green, D. H., 1979. An experimental study of the effect of Ca upon garnet-clinopyroxene Fe-Mg exchange equilibria. Contr. Miner. Petrol. 71, 13-22.

Fouch, M. J., Rondenay, S., 2006. Seismic anisotropy beneath stable continental interiors. Phys. Earth Planet. Int., 158 (2-4), 292-320.

Griffin, W. L., O'Reilly, S. Y., Ryan, C. G., 1999. The composition and origin of the subcontinental lithospheric mantle. In: Fei, Y., Bertka, C., Myson, B. O. (Eds.), Mantle Petrology: Field Observations and high-pressure experimentation: A tribute to Francis R. Boyd. Geochemical Soc. Spec. vol. 6, The geochemical Society, San Antonio, 13-45

Griffin, W. L., O'Reilly, S. Y., Doyle, B. J., Pearson, N. J., Coopersmith, H., Kivi, K., Malkovets, V., Pokhilenko, N., 2004. Lithosphere mapping beneath the North American plate. Lithos, 77, 873-922

Hayman, P.C., Cas, R.A.F., Johnson, M., 2008. Difficulties in distinguishing coherent from fragmental kimberlite: A case study of the Muskox pipe (Northern Slave Province, Nunavut, Canada). J. of Volc. Geoth. Res. 174 (2008), 139–151.

Heaman, L. M., Kjarsgaard, B. A., Creaser, R. A., 2003. The timing of kimberlite magmatism in North America: implications for global kimberlite genesis and diamond exploration. Lithos 71 (2-4), 153-184.

Heaman, L. M., Creaser, R. A., Cookenboo, H. O., Chacko, T., 2006. Multi-stage modification of the Northern Slave mantle lithosphere: evidence from zircon- and diamond-bearing eclogite xenoliths entrained in Jericho kimberlite, Canada, J. Petrology 47, 821-858.

Heaman, L. M., Pearson, D. G., 2010. Nature and evolution of the Slave Province subcontinental lithospheric mantle. Can. J. Earth Sci., 47, 369-388.

Helmstaedt H., 2009. Crust–mantle coupling revisited: The Archean Slave craton, NWT, Canada Lithos 112S, 1055–1068.

Hoffman, P. F., 1989. Precambrian geology and tectonic history of North America. In: Bally, A.W., Palmer, A.R. (Eds.), The Geology of North America - An Overview. Geological Society of America, Boulder, Colorado, 447–512.

Jacob, D. E., 2004. Nature and origin of eclogite xenoliths from kimberlites. Lithos 77 (1-4), 295-316.

Janney, P. E., Shirey, S. B., Carlson, R. W., Pearson, D. G., Bell, D. R., Le Roex, A. P., Ishikawa, A., Nixon, P. H., and Boyd, F. R., 2010. Age, composition and thermal characteristics of South African off-craton mantle lithosphere: Evidence for a multi-stage history. J of Petrology, 51, 1849-1890

Jerde, E. A., Taylor, L. A., Crozaz, G., Sobolev, N. V., 1993a. Exsolution of garnet within clinopyroxene of mantle eclogites - major-element and trace-element chemistry. Contrib Mineral Petrol 114 (2), 148-159.

Jerde, E. A., Taylor, L. A., Crozaz, G., Sobolev, N. V., Sobolev, V. N., 1993b. Diamondiferous eclogites from Yakutia, Siberia - evidence for a diversity of protoliths. Contrib Mineral Petr. 114 (2), 189-20.2

Jones, A. G., Ferguson, I. J., Chave, A.D., Evans, R.L., McNeice, G. W., 2001. Electric lithosphere of the Slave craton. Geology 29, 423–426.

Kennedy, C. S., Kennedy, G. C., 1976. The equilibrium boundary between graphite and diamond. J. of Geoph. Res. - Solid Earth 81, 2467 -2470.

Kopylova, M. G., Russell, J. K., Cookenboo, H., 1999a. Mapping the lithosphere beneath the north central Slave craton. In: Gurney, J.J., Gurney, J.L., Pascoe, M.D., Richardson, S.H. (Eds.), 7th International Kimberlite Conference, Red Roof Design cc, Capetown, 468-479.

Kopylova, M. G., Russell, J. K., Cookenboo, H., 1999b. Petrology of peridotite and pyroxenite xenoliths from the Jericho kimberlite: Implications for the thermal state of the mantle beneath the Slave craton, Northern Canada. J. Petrol 40 (1), 79-104.

Kopylova, M. G., Caro, G., 2004. Mantle xenoliths from the Southeastern Slave craton: Evidence for chemical zonation in a thick, cold lithosphere. J. Petrol 45 (5), 1045-1067.

Kopylova, M. G., Lo, J., Christensen, N. I., 2004. Petrological constraints on seismic properties of the Slave upper mantle (Northern Canada). Lithos 77 (1-4), 493-510.

Kopylova, M. G., Hayman, P., 2008. Petrology and textural classification of the Jericho kimberlite, northern Slave Province, Nunavut, Canada. Can. J. of Earth Sci., 45, 701-723.

Lallemand, S., Heuret, A., Boutelier, D., 2005. On the relationships between slab dip, back-arc stress, upper plate absolute motion, and crustal nature in subduction zones. Geochemistry Geophysics Geosystems 6, Article Number Q09006

Leake, B. E., Woolley, A. R., Arps, C. E. S., Birch, W. D., Gilbert, M. C., Grice, J. D., Hawthorne, F. C., Kato, A., Kisch, H. J., Krivovichev, V. G., Linthout, K., Laird, J., Mandarino, J. A., Maresch, W. V., Nickel, E. H., Rock, N. M. S., Schumacher, J. C., Smith, D. C., Stephenson, N. C. N., Ungaretti, L., Whittaker, E. J. W., Guo, Y. Z., 1997. Nomenclature of amphiboles: Report of the subcommittee on amphiboles of the International Mineralogical Association, commission on new minerals and mineral names. Amer. Miner. 82 (9-10), 1019-1037.

Lee, C. T., A., Luffi, P., Chin, E. J., 2011. Building and destroying continental mantle. Annual

Reviews of Earth and Planetary Sciences, 39, 59-90.

McLean, H., Banas, A., Creighton, S. et al. 2007. Garnet xenocrysts from the Diavik mine, NWT, Canada: composition, color, and paragenesis. Canadian Mineralogist, 45, 5, 1131-1145

Menzies, A., Westerlund, K., Grutter, H., Gurney, J., Carlson, J., Fung, A., Nowicki, T., 2004. Peridotitc mantle xenoliths from kimberlites on the Ekati Diamond Mine property, N.W.T., Canada: major element compositions and implications for the lithosphere beneath the central Slave craton, Lithos 77, 395-412.

Mercier, J.-P., Bostock, M. G., Audet, P., Gaherty, J. B., Garnero, E. J., Revenaugh, J., 2008. The teleseismic signature of fossil subduction: Northwestern Canada. J Geophys Res 113, B04308.

Jed L. Mosenfelder, Paul D. Asimow, Daniel J. Frost, David C. Rubie, and Thomas J. Ahrens, 2009. The MgSiO3system at high pressure: Thermodynamic properties of perovskite, postperovskite, and melt from global inversion of shock and static compression data. J Geophys. Res., 114, B01203, doi 10.1029/2008JB005900

Nakamura, D., 2009. A new formulation of garnet-clinopyroxene geothermometer based on accumulation and statistical analysis of a large experimental data set, J. of Metam. Geol. 27, 495-508.

Neal, C. R., Taylor, L. A., Davidson, J. P., Holden, P., Halliday, A. N., Nixon, P. H., Paces, J. B., Clayton, R. N., Mayeda, T. K., 1990. Eclogites with oceanic crustal and mantle signatures from the Bellsbank kimberlite, South Africa, 2. Sr, Nd, and O isotope geochemistry. Earth Planet Sc Lett 99 (4), 362-379.

Newton, D. E., Kopylova, M. G., Burgess, J., Strand, P., 2015. Peridotite and pyroxenite xenoliths from the Muskox kimberlites, northern Slave craton, Canada. Canadian Journal of Earth Sciences, in print.

Pearson, N. J., Griffin, W. L., Doyle, B. J., O'Reilly, S. Y., van Achterbergh, E., Kivi, K., 1999. Xenoliths from kimberlite pipes of the Lac de Gras area, Slave Craton, Canada. 7th Int Kimb Conf. Red Roof Design CC, Cape Town, South Africa, 644–658.

Pearson, D. G. and Nowell, G. M., 2002. The continental lithospheric mantle: characteristics and significance as a mantle reservoir. Phil. Royal. Soc. London, 360, 2383-2410

Pearson D. G., Wittig, N., 2008. Formation of Archaean continental lithosphere and its diamonds: the root of the problem. J. of the Geol. Soc., London, 165, 895–914.

Pearson, D. G. Mather, K.A., Kjarsgaard, B. Liu, J., Kopylova, M.. Dale, C., Armstrong, J., Irvine, G. 2015. The complex history of the Slave Craton lithospheric mantle root in the context of regional tectonics, Abstract, GAC-MAC-AGU

Pollack HN, Chapman DS (1977) On the regional variation of heat flow, geotherms, and lithospheric thickness. Tectonophysics 38(3):279–296

Riches, A. J. V., Liu, Y., Day, J. M. D., Spetsius, Z. V. C, Taylor, L. A., 2010. Subducted oceanic crust as diamond hosts revealed by garnets of mantle xenoliths from Nyurbinskaya, Siberia. Lithos 120, 368–378.

Rudnick, R. L., and Nyblade, A. A., 1999. The thickness and heat production of Archean lithosphere, constraints from xenolith thermobarometry and surface heat flow. In: Fei, Y., Bertka, C., Myson, B. O. (Eds.), Mantle Petrology: Field Observations and high-pressure experimentation: A tribute to Francis R. Boyd. Geochemical Soc. Spec. vol. 6, The geochemical Society, San Antonio, N6, 3-12.

Russell, JK; Dipple, GM; Kopylova, MG., 2001. Heat production and heat flow in the mantle lithosphere, Slave craton, Canada. Physics of the Earth and Planetary Interiors, 123, 1, 27-44

Schulze, D. J., 1989. Constraints on the abundance of eclogite in the upper mantle. J. Geoph. Res., 94, 4205–4212.

Schmidberger, S. S., Heaman, L. M., Simonetti, A., Creaser, R. A., Cookenboo, H. O., 2005. Formation of Paleoproterozoic eclogitic mantle, Slave Province (Canada): Insights from in-situ Hf and U-Pb isotopic analyses of mantle zircons. Earth Planet. Sci. Lett. 240, 621-633.

Schmidberger, S. S., Simonetti, A., Heaman, L. M., Creaser, R. A., Whiteford, S., 2007. Lu-Hf, in-situ Sr and Pb isotope and trace element systematics for mantle eclogites from the Diavik diamond mine: Evidence for Paleoproterozoic subduction beneath the Slave craton, Canada. Earth Planet. Sci. Lett. 254, 55-68.

Shirey, S. B., Harris, J. W., Richardson, S. H., Fouch, M., James, D. E., Cartigny, P., Deines, P., Viljoen, F., 2003. Regional patterns in the paragenesis and age of inclusions in diamond, diamond composition, and the lithospheric seismic structure of Southern Africa. Lithos 71 (2-4), 243-258.

Smart, K. A., Heaman, L. M., Chacko, T., Simonetti, A., Kopylova, M., Mah, D., Daniels, D., 2009. The origin of high- MgO diamond eclogites from the Jericho kimberlite, Canada. Earth Planet. Sci. Lett. 284, 527-537.

Smart, K. A., Chacko, T., Stachel, T., Tappe, S., Stern, R. A., Ickert, R. B., EIMF (2012). Eclogite formation beneath the northern Slave craton constrained by diamond inclusions: Oceanic lithosphere origin without a crustal signature. Earth and Planetary Science Letters 319-320, 165-177.

Smart, K. A. Chacko T., Simonetti, A., Sharp Z. D., Heaman, L. M., 2014. A Record of Paleoproterozoic subduction preserved in the Northern Slave cratonic mantle: Sr-Pb-O isotope and trace-element investigations of eclogite xenoliths from the Jericho and Muskox kimberlites. J of Petrology, 55, 3, 549-583.

Snyder, D. B., Rondenay, S., Bostockc, M. G., Lockhart, G. D., 2004. Mapping the mantle lithosphere for diamond potential using teleseismic methods. Lithos 77, 859– 872.

Snyder, D. B., and Bruneton, M., 2007, Seismic anisotropy of the Slave craton, NW Canada, from joint interpretation of SKS and Rayleigh waves, Geophys. J. Int, doi:10.1111/j.1365-246X.2006.03287.

Snyder, D. B., 2008. Stacked uppermost mantle layers within the Slave craton of NW Canada as defined by anisotropic seismic discontinuities. Tectonics, 27, TC4006, doi:10.1029/2007TC002132

Snyder, D. B., M. J. Hillier, B. A. Kjarsgaard, E. A. de Kemp, and J. A. Craven, 2014, Lithospheric architecture of the Slave craton, northwest Canada, as determined from an interdisciplinary 3-D model, Geochem. Geophys. Geosyst., 15, 1895– 1910, doi:10.1002/2013GC005168.

Snyder, G. A., Taylor, L. A., Crozaz, G., Halliday, A. N., Beard, B. L., Sobolev, V. N., Sobolev, N. V. 1997. The origins of Yakutian eclogite xenoliths. J. Petrol 38 (1), 85-113.

Sobolev, V. N., McCammon, C. A., Taylor, L.A., Snyder, G. A., Sobolev, N. V., 1999. Precise Mossbauer milliprobe determination of ferric iron in rock forming minerals and limitations of electron microprobe analysis. Amer. Mineral. 84, 78-85

Stachel, T., Harris, J. W., 2008. The origin of cratonic diamonds – Constraints from mineral inclusions. Ore Geology Reviews, 1-2, 34, 5-32. er

Taylor, L. A., Neal, C. R., 1989. Eclogites with oceanic crustal and mantle signatures from the Bellsbank kimberlite, South Africa. Part I: mineralogy, petrography and whole rock chemistry. J. Geol. 97, 551-567.

Westerlund, K. J., Shirey, S. B., Richardson, S. H., Carlson, R. V., Gurney, J. J., Harris, J. W., 2006. A subduction wedge origin for Paleoarchean peridotitic diamonds and harzburgites from the Panda kimberlite, Slave craton: evidence from Re-Os isotope systematics. Contr. Miner. Petrol. 152, 3, 275-294.

Woodland, A., Ross, C., 1994. A crystallographic and Mössbauer spectroscopy study of Fe. Phys Chem Miner 21 (3), 117–132.

Yuan, H., B. Romanowicz, K. M. Fischer, and D. Abt (2011), 3-D shear wave radially and azimuthally anisotropic velocity model of the North American upper mantle, Geophys. J. Int., 184, 1237–1260.

Figure Captions

Fig. 1. A schematic map of the Slave craton and the geology of of the surrounding terranes (Hoffmann, 1989; Helmsteadt, 2009). The line of the cross-section from the Jericho and Muskox kimberlite in the northwest to kimberlites of the Ekati and Diavik mines in the southeast is shown in red. Red dots are kimberlites of the Northern and Central Slave (Helmsteadt, 2009). The W-E line corresponds to the cross-section through the cratonic lithosphere between Wopmay orogen and Thelon front magmatic zone (TMZ) of Fig. 10B. M is the position of the McKay Lake seismic station (Snyder, 2008).

Fig 2. Macroscopic textures of eclogite xenoliths from Jericho and Muskox. (A) Massive Jericho eclogite. (B) Foliated Jericho eclogite with brown biotite-phlogopite grains. (C) Massive Jericho eclogite with abundant black rutile grains. (D-E) Foliated Muskox eclogite; white alteration of clinopyroxene is fine-grained chlorite-serpentine. (F-G) Massive Muskox eclogite, with black rutile (F) and the texture typical for diamondiferous samples (G). Black scale bars = 1 cm.

Fig 3. Microscopic textures of eclogite xenoliths from Jericho and Muskox. (A) Sample LGS1 Mx1 shows typical partial melting textures along grain boundaries of touching clinopyroxene grains. (B) A rutile grain with partial melting along the margin is recrystallized in the secondary euhedral fine grains of rutile and ilmenite and surrounded by secondary carbonate and phlogopite (sample JD40 Mx103). (C) Garnet with apatite inclusion is altered along a grain boundary to hornblende, phlogopite, opaques, and serpentine (sample LGS035 Mx4). (D) Secondary amphibole, carbonate, opaques, and phlogopite replacing garnet in sample MOX7 53.9. All images are in PPL with a FOV = 4.35 mm.

Figure 4. MgO (wt. %) vs. CaO (wt. %) for garnet from Jericho (A) and Muskox (B) eclogites with massive and foliated textures. Smaller samples with unclear texture are labeled “undetermined”. Jericho analyses are from this work and from Heaman et al., (2006), Smart et al., (2009; 2014), Kopylova et al., (1999a), and Kopylova et al. (2004). Fields A, B and C are for

distinct geological groups of eclogites according to Taylor and Neal, (1989). Open field outlines analyses from the Central Slave eclogites, i.e. from Aulbach et al., (2007), Schmidberger et al., (2007), Pearson et al., (1999), and Aulbach et al., (2011).

Fig. 5. Al_2O_3 (wt. %) vs. Na_2O (wt. %) for clinopyroxene from Jericho (A) and Muskox (B) eclogites with massive and foliated textures. Smaller samples with unclear texture are labeled "undetermined". Jericho analyses are from this work and from Heaman et al., (2006), Smart et al., (2009; 2014), Kopylova et al., (1999a), and Kopylova et al., (2004). Fields A, B and C are for distinct geological groups of eclogites according to Taylor and Neal, (1989). Open field outlines analyses from the Central Slave eclogites, i.e. from Aulbach et al., (2007), Schmidberger et al., (2007), Pearson et al., (1999), and Aulbach et al., (2011).

Fig. 6. Temperature histograms for the Jericho eclogites classified in A-B-C groups (Taylor and Neal (1989) classification modified after Coleman (1965)) computed for P=50 Kb. A: Ellis and Green (1979) temperatures; B: Nakamura (2009) temperatures. Note that some eclogites could be assigned to Group B using the clinopyroxene composition and to Group C using the garnet composition, and vice versa. This mismatch was reported for other world eclogites (Jerde et al., 1993b). We assigned the eclogites to group B if either garnet or clinopyroxene plotted in the Group B field.

Fig. 7. Pressure (Beyer et al., 2015) - temperature (Nakamura, 2009) plot for 21 Slave diamondiferous eclogites. The P-T estimates are based on Jericho samples reported in this work (all diamondiferous samples from ESM1), Jericho eclogites reported in Smart et al. (2009) and Heaman et al. (2006), Muskox eclogite (sample MOX25 207 in ESM1) and two Central Slave eclogites with omphacites containing Si< 1.985 (EA002 and EA005) from Aulbach et al. (2011). Temperature errors are constant (74^{o}), while pressure errors vary according to equation (25) of Beyer et al. (2015) as a function of Si content in omphacite. Only 2 out of 7 eclogites of Aulbach et al. (2011) has omphacites with tetrahedral Al amenable to the barometry; these are labeled with circles inside open squares. The Nakamura univariant P-T line for sample EA005 (double red line) transects the C Slave geotherm at ~ 58 kb, but intersects the Beyer et al. (2015) barometric solution at 83 kb and 1384^{o}C, exemplifying the difference in the depth placement of

eclogites related to the use of the Beyer et al. (2015) barometer. Also shown are model geotherms with 35, 40 and 45 mW/m^2 of Pollack and Chapman (1977), the Brey and Köhler (1990) Jericho geotherm (Kopylova et al., 1999b) (line with longer dashes), the Brey and Köhler (1990) Central Slave geotherm (Menzies et al., 2004) (line with shorter dashes), and the diamond stability field (Kennedy and Kennedy, 1976).

Fig. 8. The depth distribution for eclogites of groups A, B and C (Coleman, 1965; Taylor and Neal, 1989) for Jericho, Muskox and Central Slave. The depth is computed as the intersection of the Nakamura (2009) univariant P-T line for the sample with the Brey and Köhler (1990) Jericho geotherm (Kopylova et al., 1999) for Jericho and Muskox and with the Central Slave geotherm (Menzies et al., 2009) for C. Slave eclogites. Green colour marks Group A eclogites, yellow – Group B, red – Group C.

Fig. 9. The depth distribution for Jericho (A), Muskox (B) and Central Slave eclogites (C) with the inferred crustal and mantle origin. The depth is computed as the intersection of the Nakamura (2009) univariant P-T line for the sample with the Brey and Kohler (1990) Jericho geotherm (Kopylova et al., 1999b) for Jericho and Muskox and with the Central Slave geotherm (Menzies et al., 2004) for Central Slave eclogites. For Jericho and Muskox, the crustal origin is ascribed to foliated eclogites (plotted with a lighter yellow colour), whereas the mantle origin is ascribed to massive eclogites (plotted with a darker green colour); samples with undetermined textures are not shown. Only eclogites with the inferred crustal origin, i.e. all Diavik eclogites studied by Schmidberger et al., (2007), Diavik eclogites containing high-Mg and high-Ca garnets (Aulbach et al., 2007) and Ekati diamondiferous eclogites reported in Aulbach et al., (2011) are plotted for C. Slave (light yellow). The red dashed lines indicate the pressure at which the local Slave geotherms enter the diamond stability field (Kennedy and Kennedy, 1976).

Fig. 10. Cross-section through the Slave lithosphere and depth distribution of crustal eclogites beneath the Northern and Central Slave mantle. The line of the cross-section from the Jericho and Muskox pipes in the northwest to the Ekati and Diavik pipes in the southeast is shown in red on the geological map of the Slave province of Fig. 1. Depth histograms (A) are based on

massive eclogites for Jericho and Muskox pipes and for eclogites with inferred subduction origin for the Central Slave pipes. The vertical and horizontal scales for the cross-section are identical. B: A cross-section through lithosphere of Slave Province between Wopmay orogen and Thelon front magmatic zone (TMZ) along the W-E line of Fig. 1, as based on constraints from surface geology, geophysical and xenolith data (Helmsteadt, 2009). Dashed line in ultra-depleted layer (UDL) is approximate boundary between graphite (above) and diamond stability fields. Abrupt eastern boundary of Mesoarchean root at McKay Lake is thought to represent Neoarchean rifted margin. Its geometry is unconstrained, as is Neoarchean upper mantle (dark-green) to the east. K1, K2 and K3 are the Drybones Bay, Lac de Gras and Nicholas Bay kimberlites. CSMC is Central Slave Mantle Conductor of Jones et al., (2001). Age of Paleoproterozoic upper mantle to the east is from Cook and Erdmer (2005). ? denotes region that may be Neoarchean or Paleoproterozoic. H, X, and L are mantle discontinuities of Bostock (1998).

Fig. 11. Compilation of the geophysical data on the Slave craton with the depth distribution of Slave eclogites. The left column is the summary of seismic azimuthal anisotropy of the Canadian Shield (Fouch and Rondenay, 2006). The right schematic cross-section illustrating discontinuities of the Slave mantle along a ~600 km long NNW-SSE transect (modified after Snyder et al., 2014). Shown are the Moho (thick solid green line), the mid-lithosphere discontinuity (blue dashed line), Lac de Gras discontinuity (green dashed line). Mantle geometries of various terranes are con- strained by seismic discontinuities (Snyder et al., 2014). Numbers are modeled isotopic ages in Ga (Heaman and Pearson, 2010; Snyder et al., 2014). Horiszonal geochronological labels refer to peridotites, vertical labels on eclogites age estimates are maximum and minimum brackets from Table 2 of Heaman and Pearson, 2010). The lithosphere thickness (Kopylova and Caro, 2004) is constrained by the occurrence of sheared peridotites. They are present at 160 km beneath the Jericho pipe (Kopylova et al., 1999b), but are absent at depths above 210 km below Ekati (Menzies et al., 2004) and at depth above 250 km below Gahcho Kue (Kopylova and Caro, 2004). Superimposed on the cross-section is the depth distribution of Northern Slave and Central Slave crustal eclogites. The depths scales are identical for two geophysical columns and the eclogite histograms.

Table 1. Mossbauer characteristics and calculated Fe ratios for eclogitic garnet and clinopyroxene.

			Fe^{2+} in Gar					Fe^{3+} in Gar				$Fe^{3+}/\Sigma Fe$	Fe^{3+}/Σ Fe in Gar
Pipe	Classification	Sample No	QS	IS	HW1	HW2	%	QS	IS	HW	%	in Gar	corrected[1]
Jericho	Foliated Type B	JDF6N#2	3.55	1.28	0.34	0.30	97.22	0.35	0.35	0.32	2.78	0.028	0.020
Jericho	Massive Type A	JD40Mx103	3.56	1.29	0.34	0.28	91.55	0.24	0.31	0.49	8.45	0.085	0.061
Jericho	Massive Type B by Gar	LGS10Mx17	3.56	1.28	0.32	0.27	97.39	0.56	0.43	0.50	2.61	0.026	0.019
Jericho	Massive Type A	LGS25Mx11	3.56	1.29	0.31	0.27	89.48	0.42	0.28	0.46	10.52	0.105	0.076
Jericho	Foliated Type C	JD67Mx2	3.57	1.28	0.31	0.30	93.60	0.44	0.29	0.47	6.40	0.064	0.046
Jericho	Massive Type C	JD35Mx27	3.56	1.28	0.27	0.31	97.15	0.42	0.40	0.33	2.85	0.029	0.021
Jericho	Massive Type A	LGS44Mx9	3.56	1.29	0.34	0.28	89.85	0.29	0.34	0.37	10.15	0.102	0.073
Muskox	Foliated Type C	10223	3.54	1.29	0.32	0.29	94.56	0.38	0.35	0.29	5.44	0.054	0.039
Muskox	Undetermined, Type B/C	10334	3.55	1.29	0.31	0.26	94.93	0.41	0.36	0.30	5.07	0.051	0.037
Muskox	Massive, Type A/B	TRS10288	3.55	1.28	0.33	0.29	91.66	0.39	0.31	0.38	8.34	0.083	0.060
Muskox	Massive, Type B/C	10289clean	3.55	1.29	0.32	0.28	95.47	0.39	0.35	0.33	4.53	0.045	0.033
Muskox	Foliated, Type B	TRS10337	3.56	1.29	0.30	0.28	94.04	0.51	0.29	0.49	5.96	0.060	0.043
Muskox	Foliated, Type C by Gar	TRS.10283	3.54	1.28	0.32	0.27	92.52	0.45	0.35	0.39	7.48	0.075	0.054
Muskox	Massive Type B	Musc03-006	3.55	1.28	0.33	0.28	96.78	0.47	0.51	0.37	3.22	0.032	0.023

			Fe^{2+} in M1 in Cpx				Fe^{2+} in M2 in Cpx				Fe^{3+} in Cpx				$Fe^{3+}/\Sigma Fe$	T[2] for Fe total=Fe2+		T[2] for Fe3+ measured		Δ T[3]	Δ T[3]
Pipe	Classification	Sample No	QS	IS	HW1	%	QS	IS	HW1	%	QS	IS	HW	%	in Cpx	5 GPa	6 GPa	5 GPa	6 GPa	5 GPa	6 GPa
Jericho	Foliated Type B	JDF6N#2	2.72	1.15	0.36	23.39	2.05	1.16	0.55	42.45	0.50	0.39	0.50	34.16	0.342	901	948	790	833	111	115
Jericho	Massive Type A	JD40Mx103	2.69	1.15	0.32	10.22	2.00	1.16	0.42	69.79	0.56	0.36	0.49	19.99	0.199	990	1037	916	961	74	76
Jericho	Massive Type C by Cpx	LGS10Mx17	2.79	1.16	0.40	38.36	1.98	1.17	0.54	42.61	0.56	0.36	0.48	19.03	0.190	980	1026	906	949	74	77
Muskox	Foliated, Type B by Cpx	TRS.10283	2.75	1.16	0.37	30.32	1.97	1.19	0.51	33.47	0.50	0.37	0.40	36.21	0.362	1031	1084	897	944	135	140
Muskox	Massive Type B	Musc03-006	2.75	1.16	0.34	23.21	2.02	1.16	0.56	62.41	0.43	0.29	0.46	14.38	0.144	940	983	894	935	46	48

(QS) Quadrupole splitting , (IS) isomer shift, (HW1) and (HW2) half-widths of the low- and high- velocity peaks.

1 - corrected values after Woodland&Ross (1994)
2 - Nakamura (2009) temperatures
3 - the difference between the estimated temperatures corrected and not corrected for Fe^{3+}

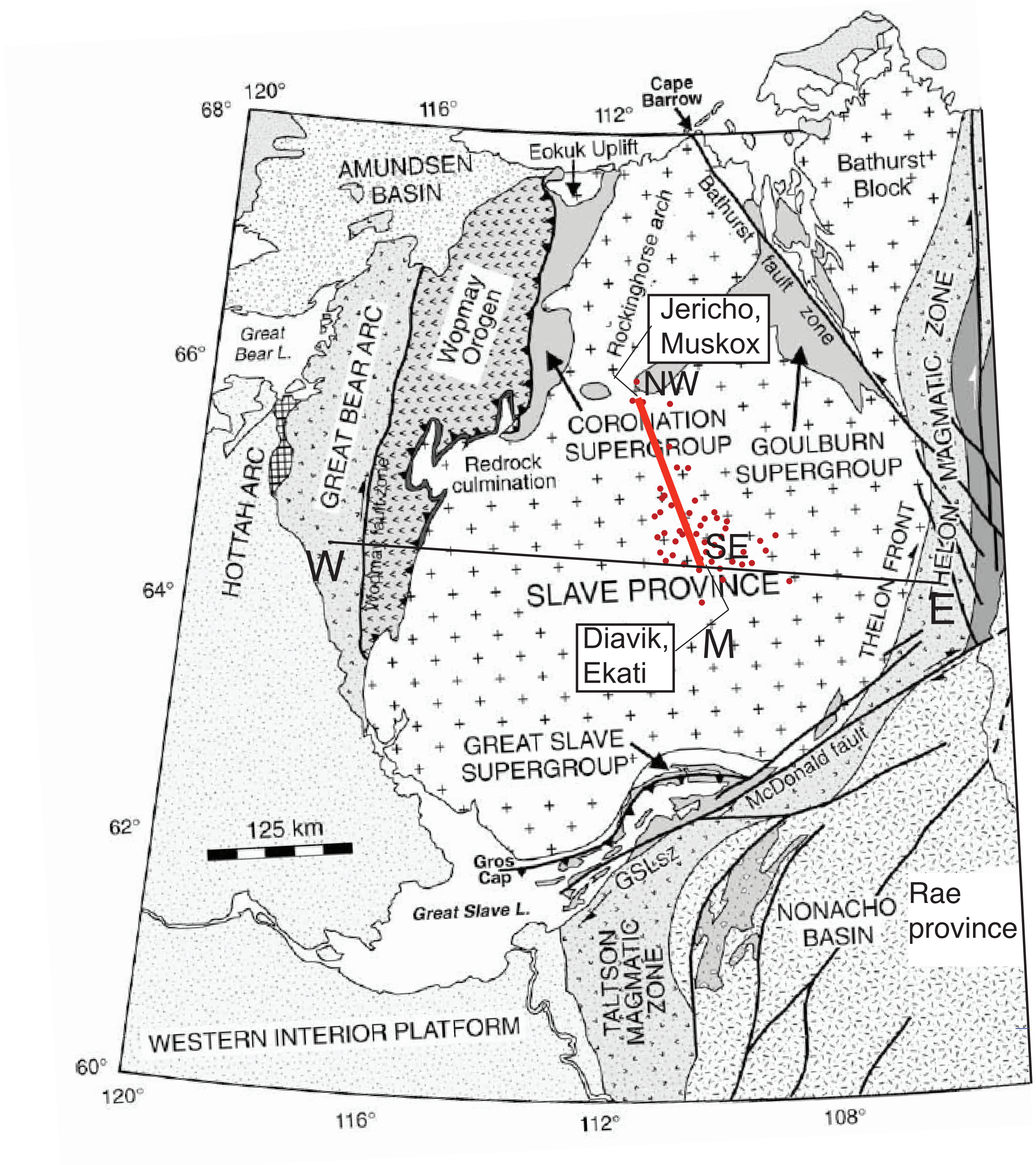

68°
120°
116°
112°
Cape Barrow
Eokuk Uplift
AMUNDSEN BASIN
Bathurst Block
Rockinghorse arch
Bathurst fault zone
Wopmay Orogen
Great Bear L.
66°
GREAT BEAR ARC
Jericho, Muskox
NW
CORONATION SUPERGROUP
GOULBURN SUPERGROUP
THELON MAGMATIC ZONE
HOTTAH ARC
Redrock culmination
W
SE
SLAVE PROVINCE
64°
THELON FRONT
E
Diavik, Ekati
M
GREAT SLAVE SUPERGROUP
McDonald fault
62°
125 km
Gros Cap
GSLsz
Great Slave L.
NONACHO BASIN
Rae province
TALTSON MAGMATIC ZONE
WESTERN INTERIOR PLATFORM
60°
120°
116°
112°
108°

Figure 1

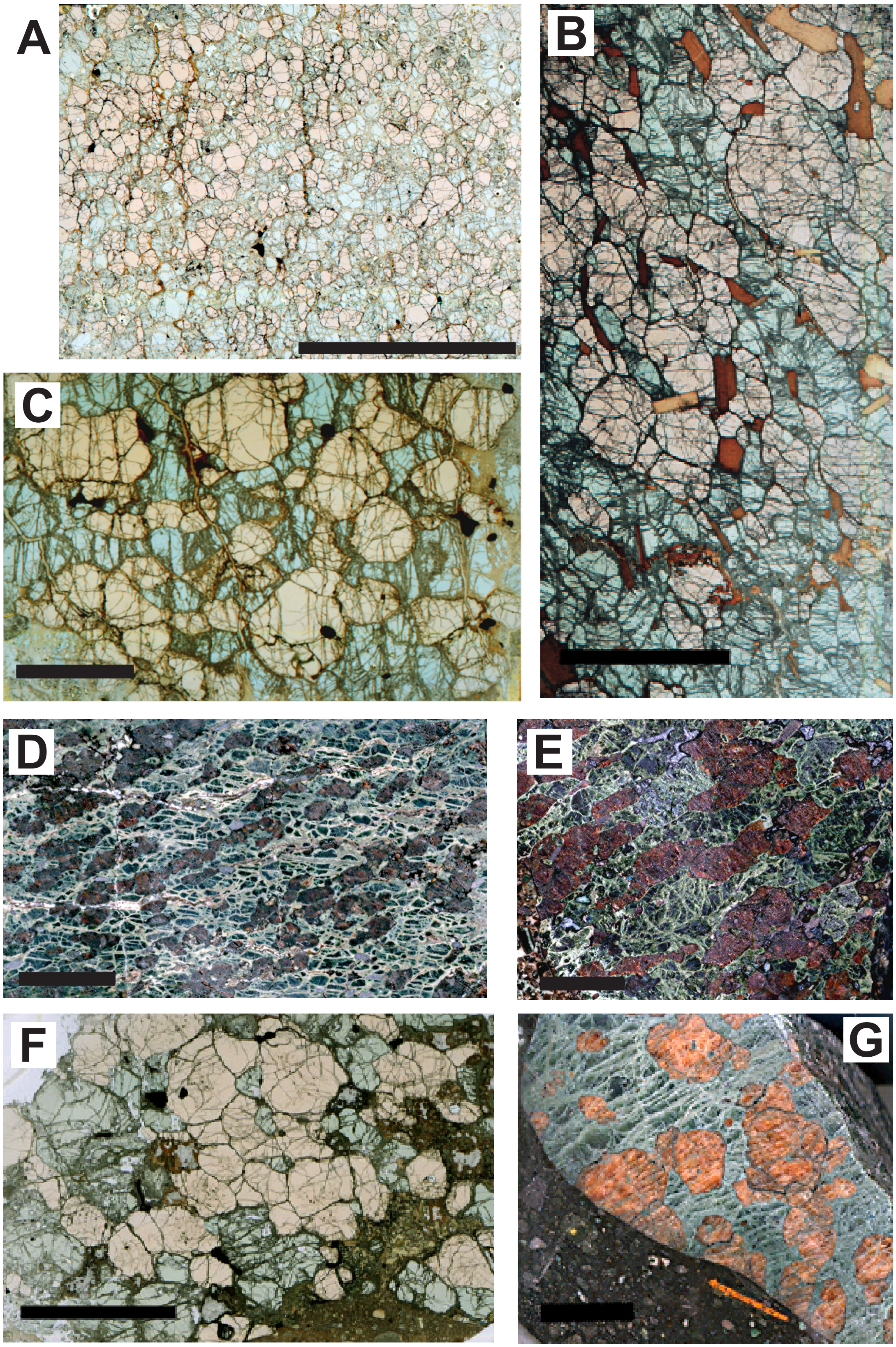

Figure 2

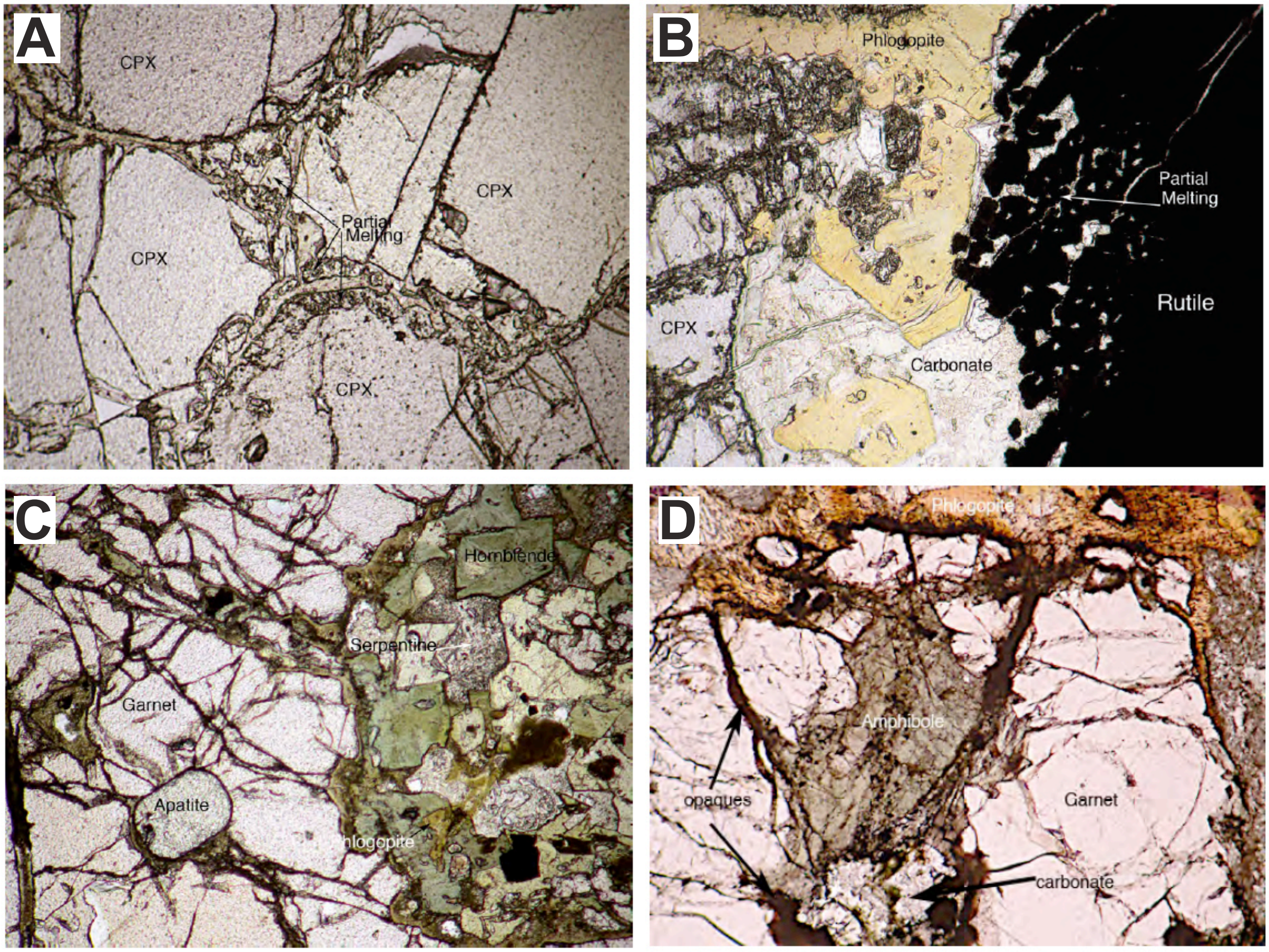
A
CPX
CPX
CPX
CPX
Partial
Melting
B
Phlogopite
Partial
Melting
Rutile
CPX
Carbonate
C
Hornblende
Serpentine
Garnet
Apatite
Phlogopite
D
Phlogopite
Amphibole
opaques
Garnet
carbonate

Figure 3

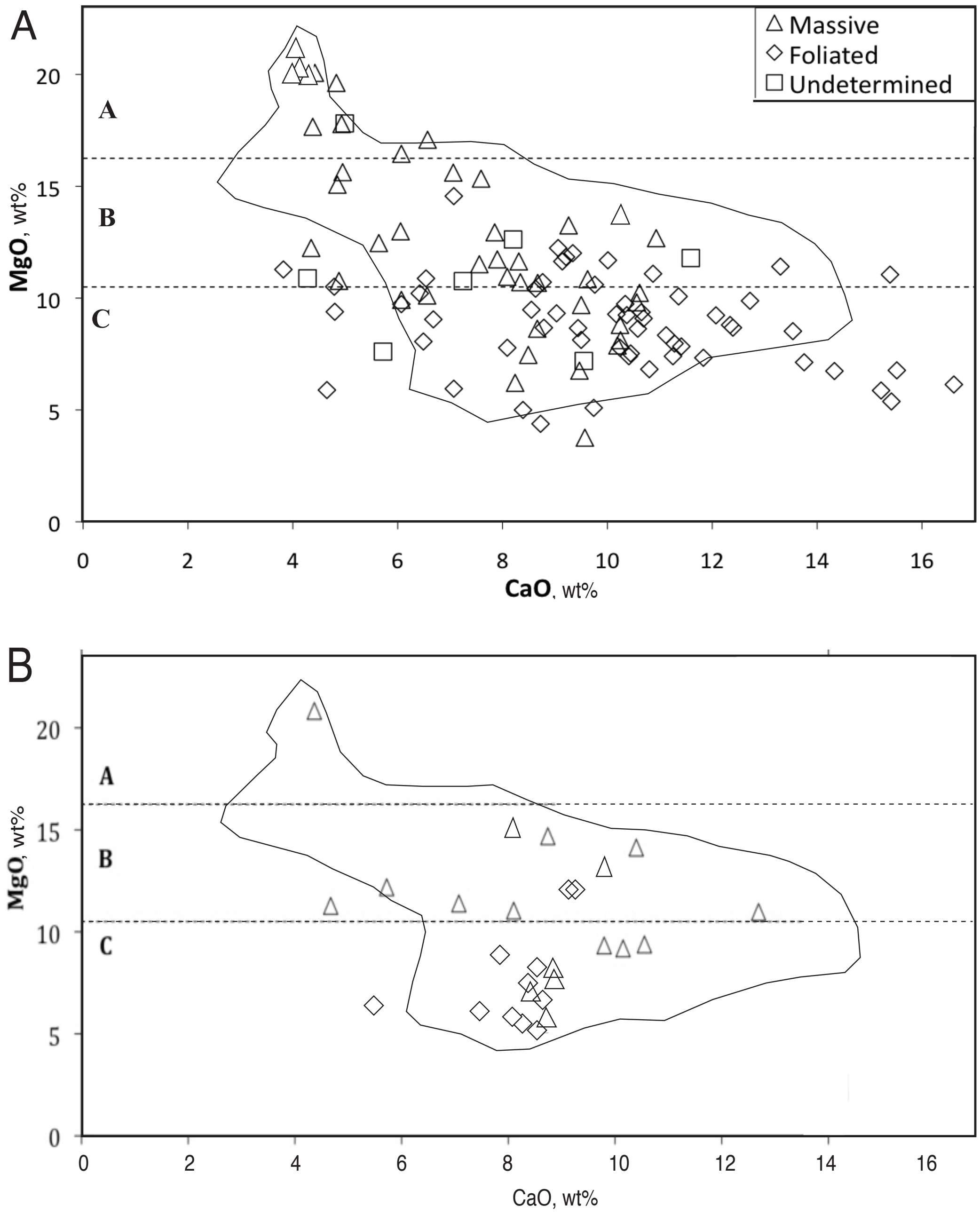
A
Massive
Foliated
Undetermined
A
B
C
MgO, wt%
CaO, wt%
0
5
10
15
20
0
2
4
6
8
10
12
14
16
B
A
B
C
MgO, wt%
CaO, wt%
0
5
10
15
20
0
2
4
6
8
10
12
14
16

Figure 4

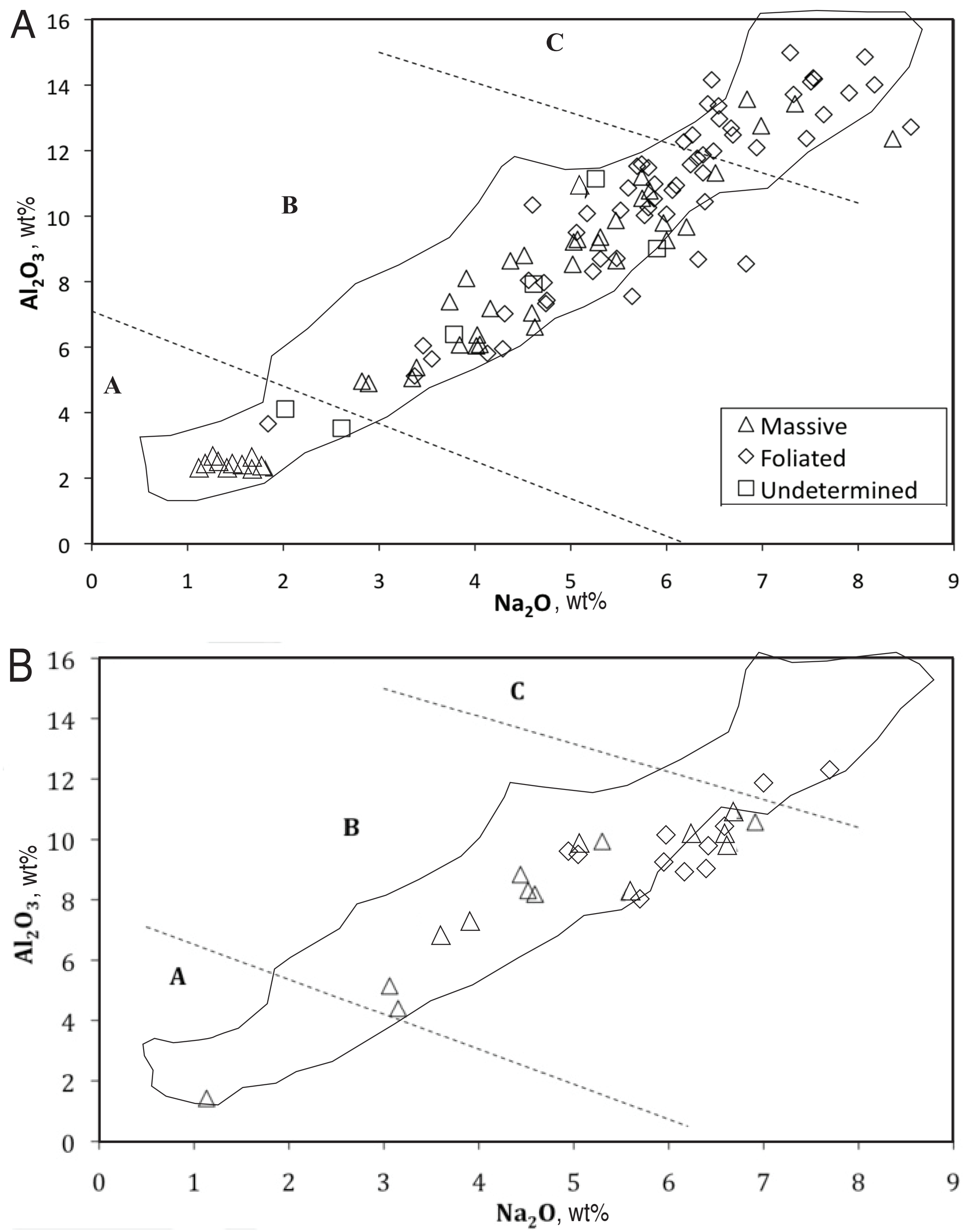
A
B
C
B
A
Al2O3, wt%
Na2O, wt%
Massive
Foliated
Undetermined
B
C
B
A
Al2O3, wt%
Na2O, wt%

Figure 5

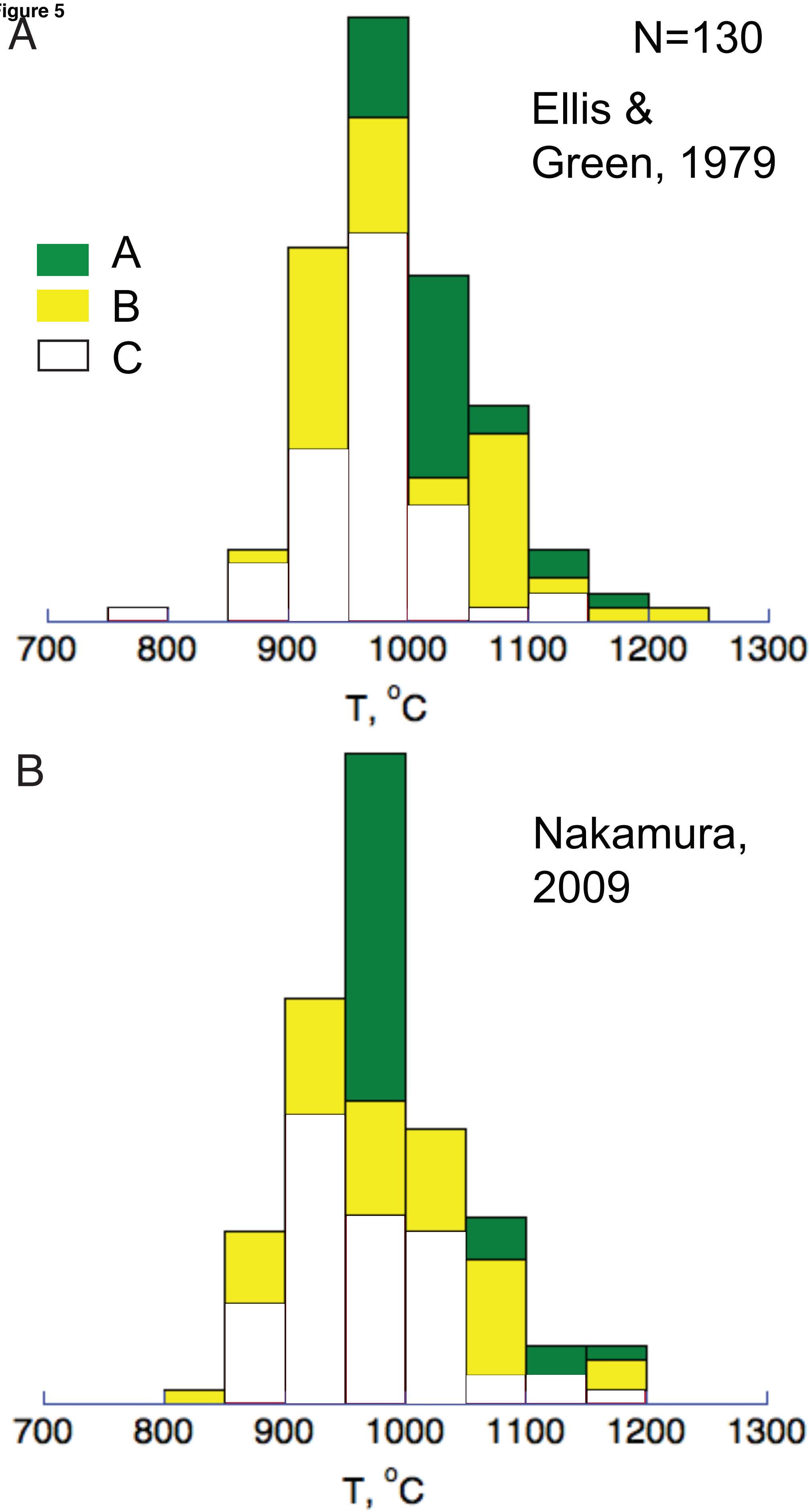
A
N=130
Ellis & Green, 1979
A
B
C
700
800
900
1000
1100
1200
1300
T, °C
B
Nakamura, 2009
700
800
900
1000
1100
1200
1300
T, °C

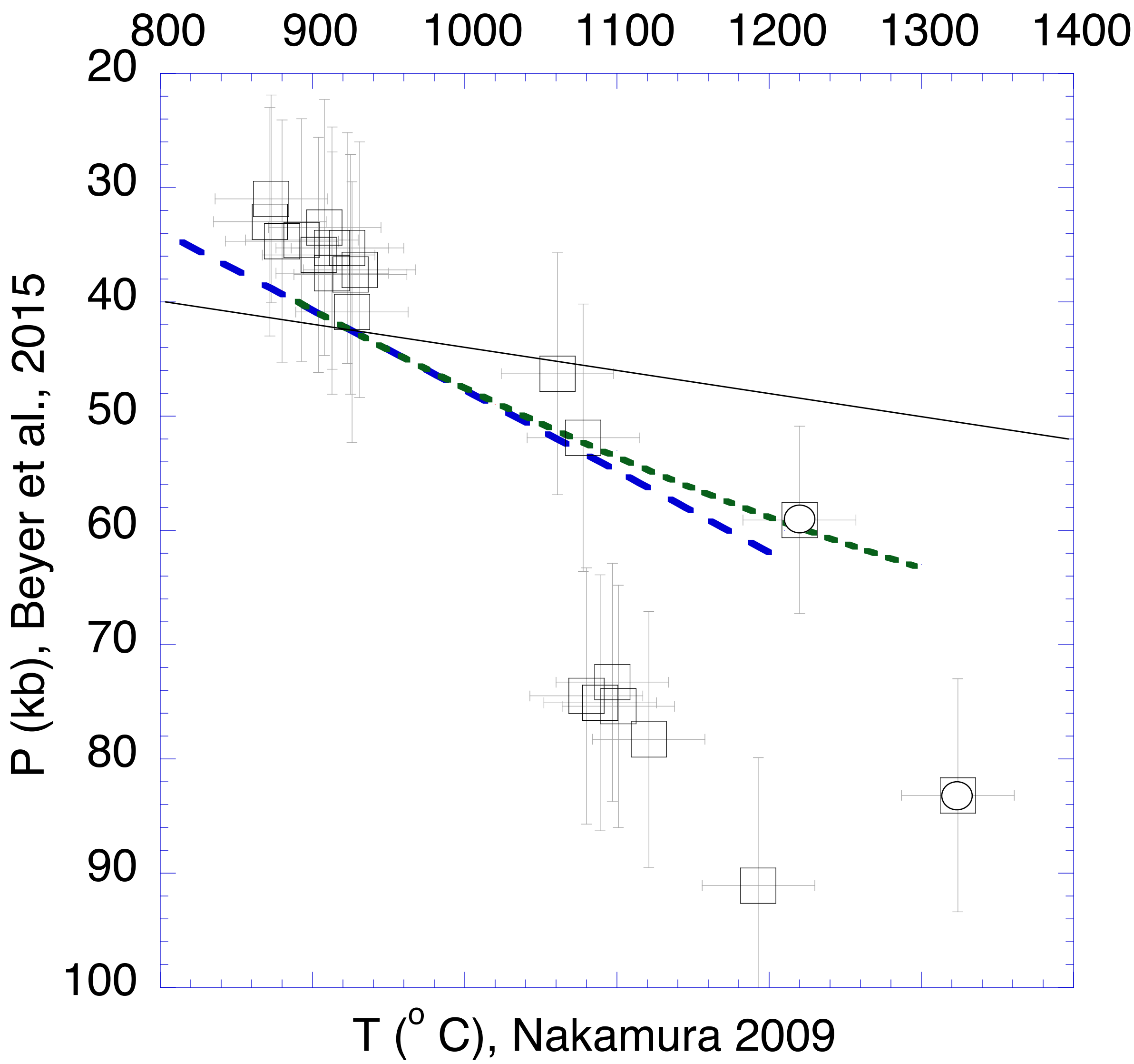
800
900
1000
1100
1200
1300
1400
20
30
40
50
60
70
80
90
100
P (kb), Beyer et al., 2015
T (o C), Nakamura 2009

Figure 6

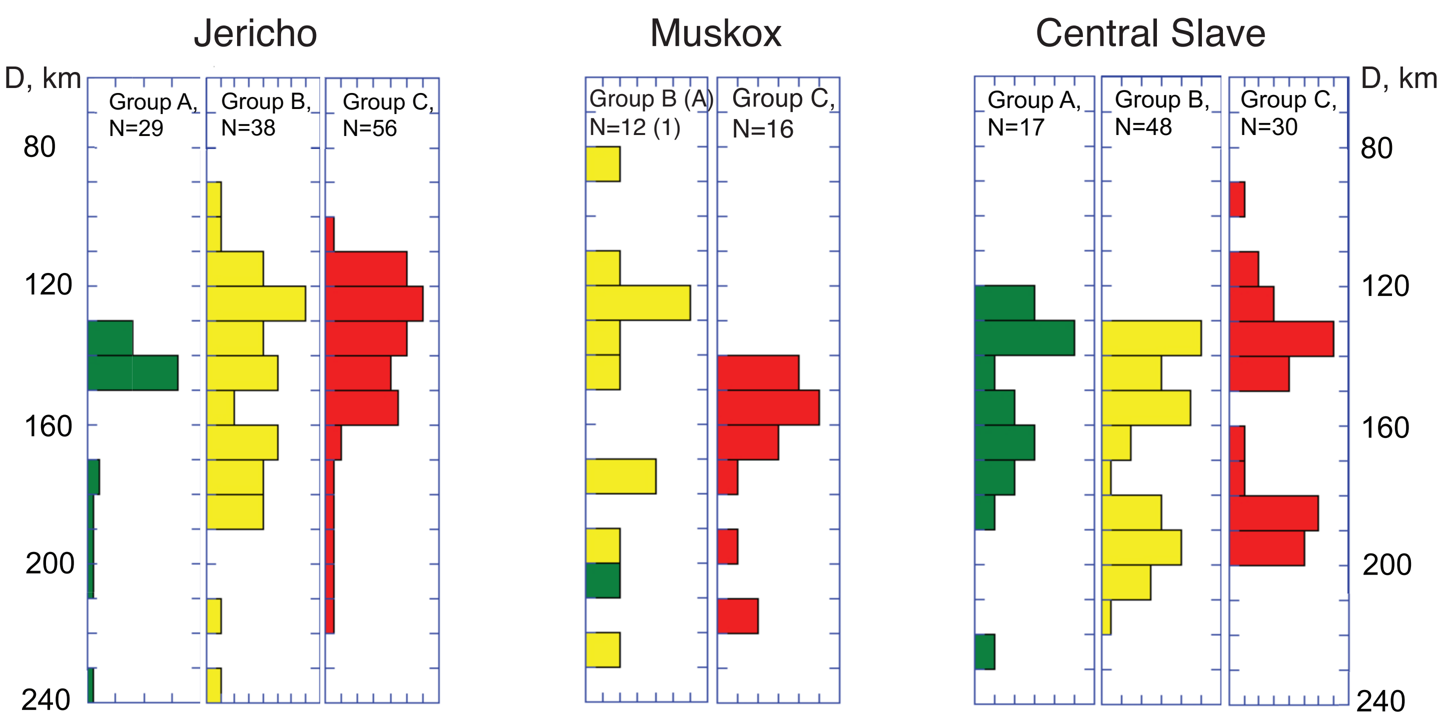
Jericho
Muskox
Central Slave
D, km
80
120
160
200
240
Group A,
N=29
Group B,
N=38
Group C,
N=56
Group B (A)
N=12 (1)
Group C,
N=16
Group A,
N=17
Group B,
N=48
Group C,
N=30
D, km
80
120
160
200
240

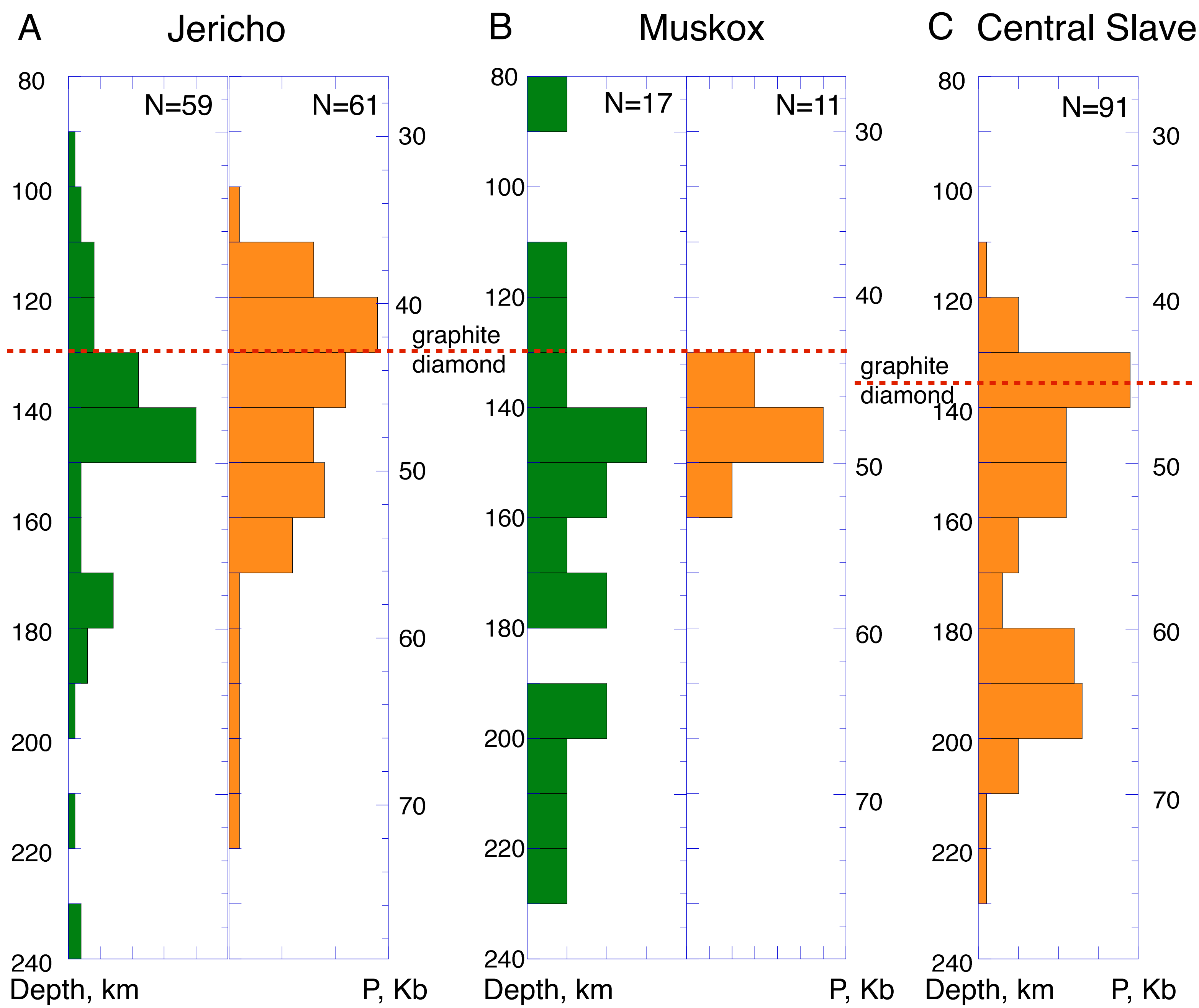

A
Jericho
N=59
N=61
B
Muskox
N=17
N=11
C
Central Slave
N=91
graphite
diamond
graphite
diamond
80
100
120
140
160
180
200
220
240
30
40
50
60
70
Depth, km
P, Kb
Depth, km
P, Kb
Depth, km
P, Kb

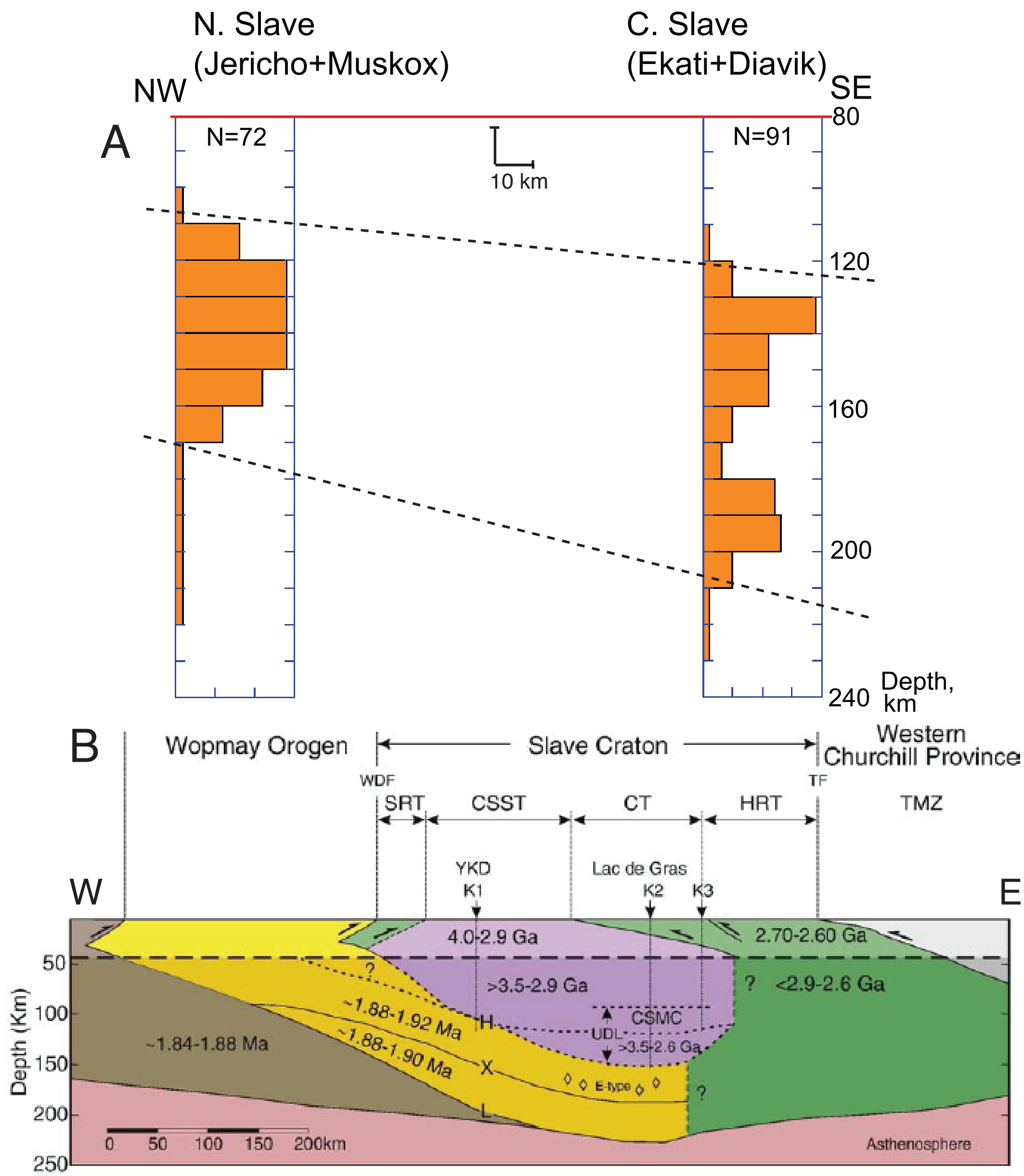

N. Slave
(Jericho+Muskox)
C. Slave
(Ekati+Diavik)
NW
SE
A
N=72
N=91
10 km
80
120
160
200
240
Depth, km
B
Wopmay Orogen
Slave Craton
Western Churchill Province
WDF
TF
SRT
CSST
CT
HRT
TMZ
YKD
K1
Lac de Gras
K2
K3
W
E
4.0-2.9 Ga
2.70-2.60 Ga
>3.5-2.9 Ga
? <2.9-2.6 Ga
CSMC
UDL
>3.5-2.6 Ga
~1.88-1.92 Ma
~1.88-1.90 Ma
~1.84-1.88 Ma
H
X
L
E-type
Depth (Km)
50
100
150
200
250
0 50 100 150 200km
Asthenosphere

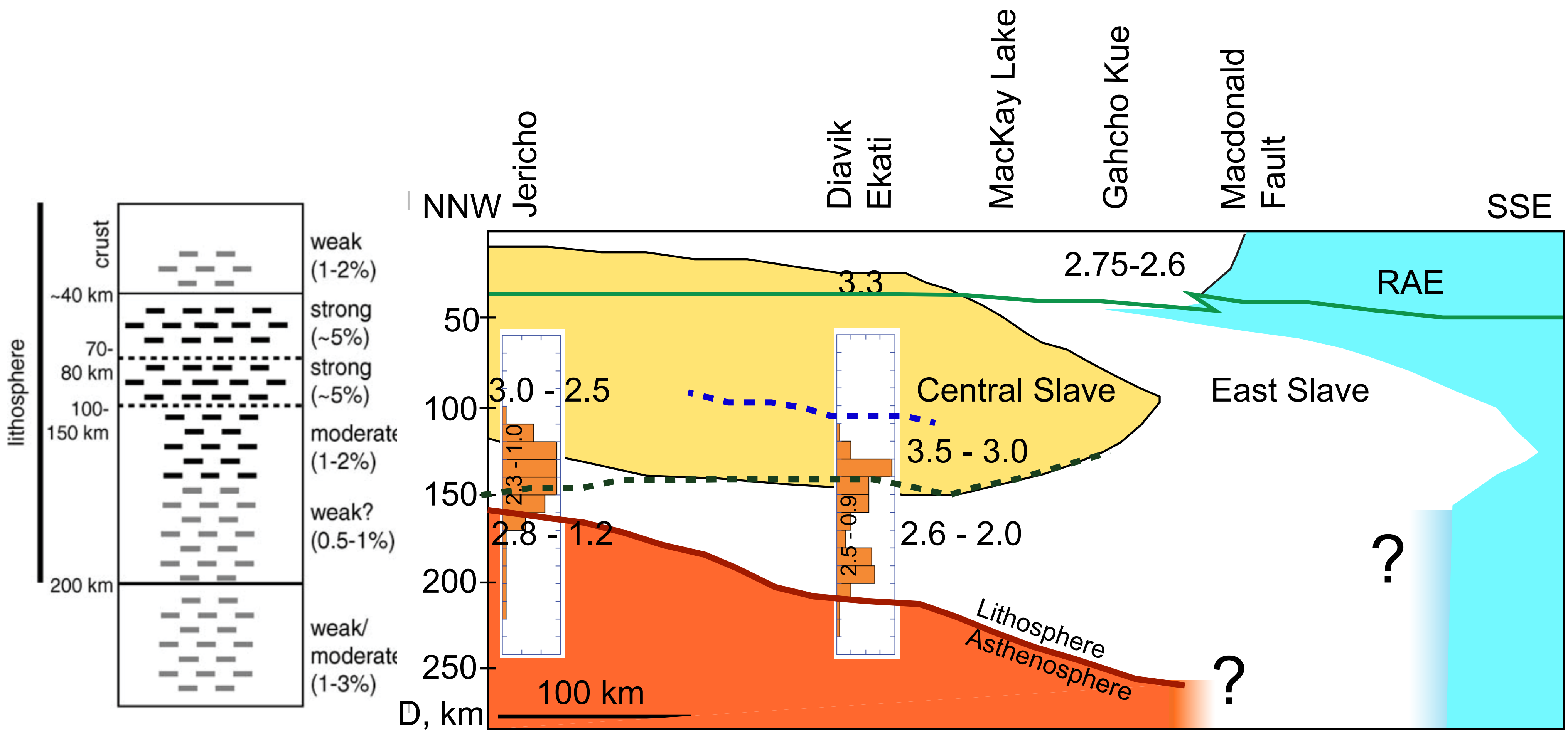

lithosphere
crust
weak
(1-2%)
~40 km
strong
(~5%)
70-
80 km
strong
(~5%)
100-
150 km
moderate
(1-2%)
weak?
(0.5-1%)
200 km
weak/
moderate
(1-3%)
NNW
Jericho
Diavik
Ekati
MacKay Lake
Gahcho Kue
Macdonald
Fault
SSE
2.75-2.6
RAE
3.3
50
100
150
200
250
D, km
3.0 - 2.5
Central Slave
East Slave
3.5 - 3.0
2.3 - 1.0
2.8 - 1.2
2.5 - 0.9
2.6 - 2.0
Lithosphere
Asthenosphere
100 km
?
?